1.0

1.1

1.25 1.4 1.6

2.8 2.5

3.2 2.2

3.6

4.0 2.0

1.8

45
50
3.6
6.3

MICROCOPY RESOLUTION TEST CHART
NATIONAL BUREAU OF STANDARDS 1963 A
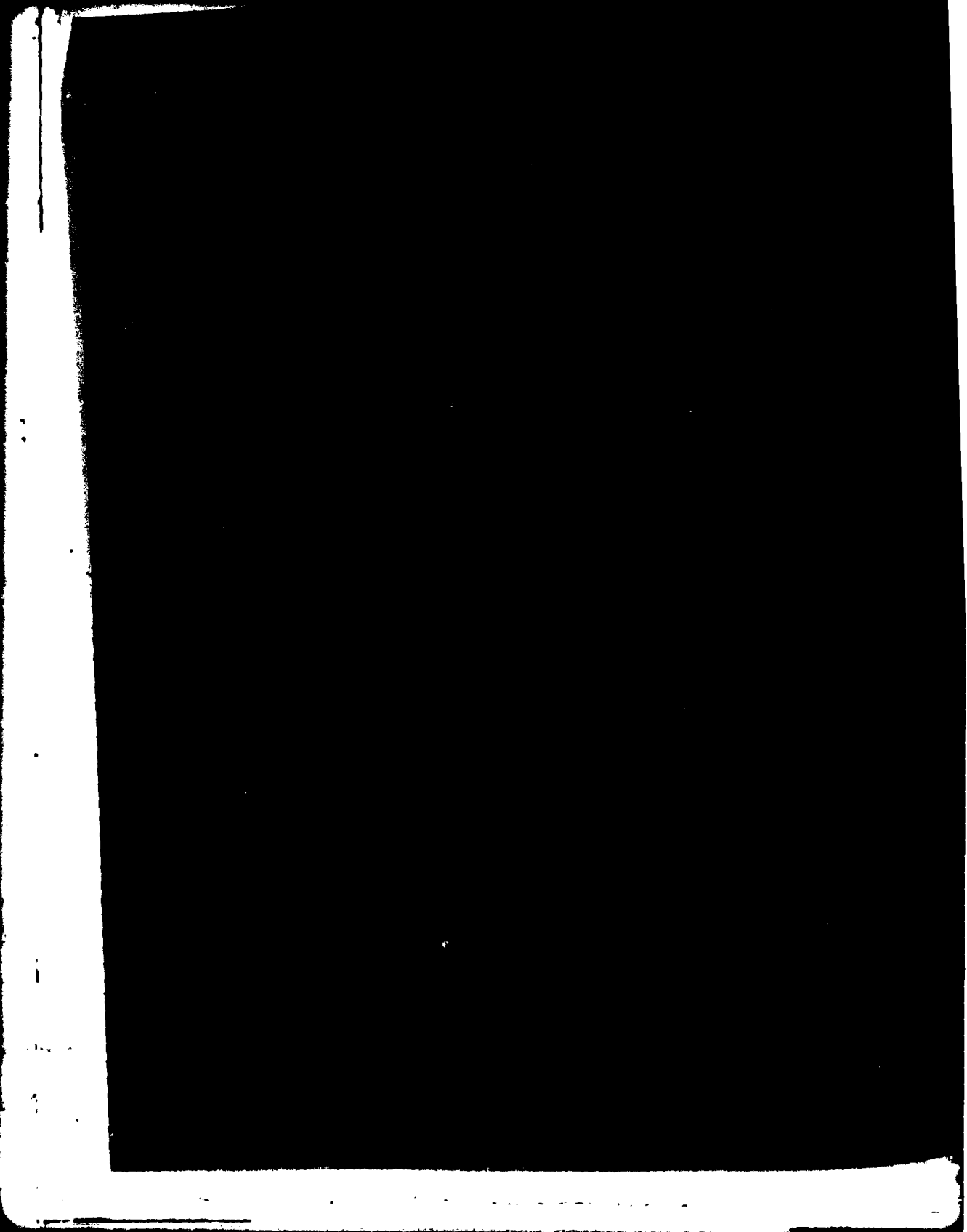
MASSACHUSETTS INSTITUTE OF TECHNOLOGY

LINCOLN LABORATORY

WIDEBAND ADAPTIVE ANTENNA NULLING
USING TAPPED DELAY LINES

J. T. MAYHAN
A. J. SIMMONS
W. C. CUMMINGS

Group 61

TECHNICAL NOTE 1979-45

26 JUNE 1979

DTIC
SELECTED
APR 8 1980

B

LEXINGTON   MASSACHUSETTS

ABSTRACT

For some applications, it is desirable to have an antenna which can adaptively form antenna pattern "nulls" in the directions of a collection of interference sources. These nulls are generally required to be below some specified level of directive gain over the entire system bandwidth. Typically the nulls are formed by adaptively weighting each output of an N-port antenna, such as an N-element array. For large arrays operating over wide percentage bandwidths, some sort of frequency compensation is required at each output port to accomplish broadband nulling. One technique commonly used is to employ a "tapped" delay line at each element output, with controllable weights (frequency independent) at the output of each tap. The objective of this report is to develop some insight into the way in which delay line compensation leads to improved performance, to develop some quantitative estimates of how performance varies with antenna and delay line parameters, and to develop some tools useful in the performance evaluation of frequency dependent weighting.

Practical considerations dictate that only a minimum number of taps/ element be utilized. A primary consideration is to minimize the number of taps required for a specific system performance. With this objective in mind, we develop an analytic solution characterizing the two element array, employing a two-tap delay line with each element. This provides valuable insight into the mechanism of delay line compensation. Results for this simple case will then be extended to the N-element planar array using N_t taps/element. That tap spacing which optimizes the array performance from the viewpoint of providing wideband nulls on sources incident on the array from locations arbitrarily specified over the antenna field of view is developed, and applied to numerous types of array configurations. The composite performance of nine specific array configurations is used to estimate the number of taps and tap spacing which would be required for an arbitrary array configuration, as a function of the array and delay line parameters $\Delta\gamma_m = 2\pi \frac{D}{\lambda} \sin\Theta_m$, FBW, ϕ_0 and N_t, where FBW is the fractional bandwidth (100*FBW = percentage nulling bandwidth) Θ_m is the maximum scan angle off broadside, ϕ_0 the tap spacing

iii

(in degrees relative to the center-band frequency) D is the maximum aperture
dimension, and N_t the number of taps. The implications of using an Applebaum-
Howells type of adaptive processor to determine the delay-line output weighting,
and the algorithm effects on performance, are also developed.

CONTENTS

ILLUSTRATIONS

vi

ILLUSTRATIONS (cont'd)

I.   INTRODUCTION

For some applications, it is desirable to have an antenna which can adaptively form antenna pattern minima, or "nulls" in the direction of a collection of interference sources. These minima are generally required to be below some specified level of directive gain over the entire system bandwidth. When this bandwidth is quite large (for example, when bandspreading is used in the modulation format of a communications signal), the level of nulling which can be achieved becomes dependent on the aperture size (in wavelengths), the antenna field of view (FOV), and the RF fractional bandwidth (FBW). Typically, such nulls are formed by adaptively weighting each of the outputs of an N-port antenna such as an N-element array, or N-beam multibeam antenna, and then summing these weighted outputs so as to form minima in the radiation pattern in the directions of the interference sources, and relative maxima in the directions of the desired users of the system. For large antennas operating over wide percentage bandwidths, some sort of frequency compensation is required at each antenna output port to accomplish broadband nulling. One technique commonly used is a frequency dependent weight consisting of a "tapped" delay line with controllable weights (frequency independent) at the output of each tap, and the weighted tap outputs summed. The net effect is to adaptively synthesize the "optimum" frequency-dependent weight at each element. Several papers have addressed this problem[1,2,3]. The objective of this report is to develop some additional insight into the way in which delay line compensation leads to improved performance, to develop some quantitative estimates of how performance varies with the antenna and delay line parameters, and to develop some tools useful in the performance evaluation of frequency dependent weighting.

Practical considerations dictate that only the minimum number of taps per element required to achieve the desired performance be utilized. For an N-element array using N_t taps (N_t=1 corresponds to frequency independent weights with no delay lines), then $N \cdot N_t$ controllable weights are required. A primary consideration is to minimize N_t required for a specific system performance. With this goal in mind, it is useful to consider the performance characteristics

of an N-element array using frequency <u>independent</u> weighting, so that the need
for incorporating the more complex delay line processor can be quantified.
Fig. 1 illustrates an estimate of the cancellation performance, using frequency
independent weighting, for an N-element linear array for the cases N=2, 7 and
17. Each array case forms N-1 nulls on N-1 interference sources separated
greater than a half-power beamwidth (HPBW) from its neighbor. For our puposes,
the cancellation C plotted in Fig. 1 is defined to be the quotient of the
interference to thermal noise ratio at the array output after nulling to that
before nulling (see Eqs. 38 and 39 of the text), when the interference is
assumed to consist of white noise over the bandwidth BW. The quiescent radia-
tion pattern of the array is assumed to be "earth coverage" (i.e., a single
array element is used as the reference element, where the element pattern
covers the earth FOV with applications pertaining to an uplink to a satellite
at geosynchronous orbit). For convenience we define the fractional bandwidth,
FBW, as BW/f_0, where f_0 is the operating frequency and BW is the nulling band-
width (in hertz). The development leading up to Fig. 1 is presented in Appen-
dix A. Referring to the figure, it is convenient to characterize the array
performance according to the variables D/λ, $\sin\Theta_m$ and FBW, where D/λ denotes
the aperture diameter in wavelengths, and Θ_m is the maximum scan angle defining
the field of view over which the array must operate. The cancellation degrades
rapidly as any of the parameters D/λ, Θ_m or FBW is increased. More precisely
$C \propto (\Delta\gamma_m \cdot FBW)^2$, where $\Delta\gamma_m \equiv 2\pi \cdot \frac{D}{\lambda} \cdot \sin\Theta_m$. If the desired cancellation
performance is specified, Fig. 1 can be used to estimate the corresponding
maximum allowable value of $\Delta\gamma_m$ consistent with this performance specification.
If system requirements dictate that a value of $\Delta\gamma_m$ greater than this maximum is
required (for example, the minimum allowable user-interference separation
dictates the choice of D/λ), frequency dependent weighting requiring $N_t > 1$
must be used. As an example of the use of Fig. 1, if we desire $C \lesssim -30$ dB,
then $\Delta\gamma_m \cdot FBW$ must be less than 0.25 if frequency independent weights are used.
For the geosynchronous satellite uplink geometry, Θ_m is fixed at approximately
9°. D/λ is determined by the user-interference resolution required. The
tolerable bandwidth with frequency independent weighting is then specified by
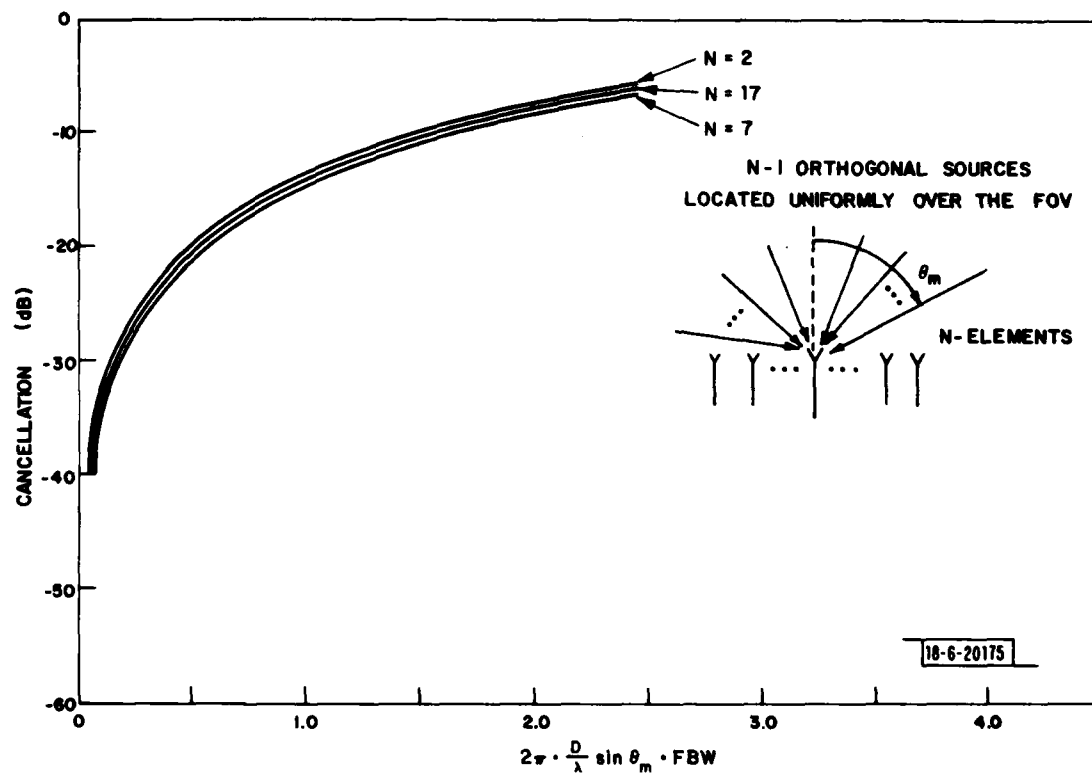
Fig. 1. Cancellation vs $2\pi \cdot \frac{D}{\lambda} \sin \Theta_m \cdot$ FBW for an N-element, equi-spaced linear array using frequency independent weighting.

3

the requirement $\Delta\gamma_m \cdot FBW \leq 0.25$. Results similar to Fig. 1 specifying the performance of the delay line processor for use with specific array configurations will be presented in Sections III and IV.

Observe from Fig. 1 that the cancellation estimates are relatively independent of the number of array elements used. It will be seen later that, in fact, the estimates of Fig. 1 serve as an upper bound on the cancellation performance of the more complex planar arrays. However, the general behavior indicating $C \alpha (\Delta\gamma_m \cdot FBW)^2$ remains valid. Only the constant of proportionality changes with array configuration. It should be pointed out, however, that this dependence is characteristic only of array antennas. For multiple beam antennas (MBA's) employing beams formed using time-delayed techniques, it can be shown that $C \alpha FBW^2$, and is relatively independent of D/λ and Θ_m. This results from the time-delayed nature of each of the beams. A detailed discussion of the MBA bandwidth behavior is presented in Ref. 4. Because of these basic differences between the MBA and the array antenna, the results characterizing the array configurations treated in the following sections cannot be directly extrapolated to the MBA.

In the following section, we will introduce several concepts which are fundamental to obtaining a quantitative assessment of the performance of adaptive antennas using a delay line processor. Direct assessment of the bandwith performance of an N-element antenna used in conjunction with an adaptive processor is difficult unless the array is required to form N-1 independent nulls. This is because the array possesses N-1 available degrees of freedom, and forming less than N-1 nulls allows the processor to compensate for any narrowband tendency inherent in the antenna by using the additional available degrees of freedom to form wide-band nulls. However, this type of wide-band null tends to be spatially broader than the corresponding narrowband case, so that the spatial resolution of the array is compromised. When a tapped delay line is used to wide-band the array, the narrowband spatial resolution of the array is preserved. To avoid this ambiguity, and to establish a basis for comparing array performance with and without a delay line processor, we introduce the concept of "orthogonal" sources. By definition, such sources use up a

4

complete degree of freedom per source to be nulled. Subjecting the array to
N-1 orthogonal interference sources necessarily requires all the available N-1
degrees of freedom of the array to be allocated to _spatial_ nulling, with none
remaining for bandwidth compensation. The improvement in performance realized
using delay line processing compared to frequency independent weighting can
then be quantitatively assessed for this type of scenario.

A second useful concept offering insight into how delay line compensation
leads to improved performance is that of "optimum weighting". The set of
optimum weights, by definition, has the precise frequency variation required to
perfectly null all the N-1 orthogonal interference sources over the entire
bandwidth of interest. The frequency dependence of these optimum weights can
readily be determined. The function of the delay line processor is to synthe-
size an effective weight variation with frequency which approximates this
optimum weight variation. The degree to which this is possible depends on the
delay line parameters i.e., the tap spacing and the number of taps. A novel
graphical presentation illustrating this synthesis of the optimum weights via
delay lines will be developed in Section II and used throughout in evaluating
the characteristics of specific antenna configurations.

The performance of an N-element adapative array is strongly dependent on
the control algorithm used in the delay line processor. In Section III we
present an analysis of this dependence assuming that an Applebaum-Howells type
adaptive feedback processor[5] controls the weights at the output of each tap
of the delay line. For this type of processor, the quiescent radiation pattern
of the array is governed by "beam-steering" controls applied to the control
loops. Upon adaption, the weights are set to a value which reduces the radia-
tion pattern in the direction of the interference sources to a minimum level
dependent on the loop gain (or processor dynamic range), while simultaneously
yielding the best rms approximation to the quiescent radiation pattern in
directions away from the interference. Choice of loop gain (i.e., the effec-
tive power level of the interference sensed by the processor) determines the
tradeoff between depth of null and rms pattern error of the adapted pattern

5

relative to the quiescent pattern. The dependence of the array performance on processor parameters will be evaluated for the two-element array using two taps/element. For this simple case, detailed analytical solutions can be obtained, providing a physical feeling for how delay line compensation improves the array nulling bandwidth. Proper choice of the steering vector required to keep the array from "turning itself off" will also be developed. It will be shown that only in the limit of very large loop gain is the full potential of the delay line processor realized.

Finally, in Section IV, the performance of specific N-element linear and planar arrays operating over a fixed FOV will be quantified as a function of $\Delta\gamma_m$, the tap spacing, number of taps and the nulling bandwidth for processors having very large loop gain. In this limit, array performance becomes independent of the control algorithm, and only dependent on the array and delay line parameters. Of prime interest will be to characterize how the cancellation over FBW improves as the number of taps increases, so that only the minimum number of taps might be used for specific system applications. The composite results determined from numerous array configurations will be used to estimate a specific value of N_t required to obtain a specified cancellation performance for an arbitrary array configuration. These results are summarized in Figs. 24a, b and c of the text.

6

II. PERFORMANCE EVALUATION CONCEPTS

A. The Concept of Orthogonal Interference Sources

As discussed in the previous section, it is useful to introduce the concept of orthogonal interference sources. By definition, such sources use up a complete degree of freedom available to the array per source to be nulled. Subjecting an N-element array to N-1 orthogonal sources necessarily requires all the available N-1 degrees of freedom of the array to be allocated to spatial nulling, with none remaining for bandwidth compensation. Mathematically, this condition can be stated as follows:

Define the source direction vector $\underline{u}$, whose components are the outputs of each element of the array when a _narrowband_ signal of unit amplitude from direction Θ, ϕ is incident on the aperture, according to

$$(\underline{u})_k = e^{+jk_0 \frac{D}{2} \sin\Theta (x_k \cos\phi + y_k \sin\phi)}, \quad k=1, \ldots, N \tag{1}$$

where $k_0 = 2\pi/\lambda = \omega_0/c$, λ is the wavelength, ω_0 the operating frequency, $c = 3\times10^8$ m/sec, D the diameter of the circle circumscribing the array, Θ, ϕ the angular coordinates specifying the source direction relative to array broadside, and the x_k, y_k are the normalized (relative to D/2) element placement coordinates ($x_k^2 + y_k^2 \leq 1$). Hence, when $\underline{u}^\dagger$ is applied to the array elements as a weight vector, then the array output response is maximum. (Note: "$\dagger$" denotes "complex conjugate transpose.") A set of orthogonal sources at positions $\underline{u}_i$, $\underline{u}_j$ satisfies the orthogonality conditions

$$\underline{u}_i^\dagger \cdot \underline{u}_j = N\delta_{i,j} \quad i,j = 1, \ldots, N \tag{2}$$

where $\delta_{i,j}$ denotes the Kronecker delta function ($\delta_{i,j} = 0$, $i \neq j$; $\delta_{i,j} = 1$, $i = j$). Physically this occurs when the sources are sufficiently far apart so that a separate null (other than a grating lobe null) is required for each. At least one set of sources satisfying (2) can be found for most arrays of

7

interest, and a set which at least approximately satisfies (2) can be found for all arrays.

Consider then J narrowband incoherent interference sources emanating from the directions Θ_j, ϕ_j, $j=1, \ldots, J$. The correlation matrix characterizing the array element voltage outputs, E_k, is given by

$$\underline{\underline{R}}_A = E \left\{ E_k E_q^* \right\} = R_1 G_e \underline{u}_1 \underline{u}_1^+ + \ldots + R_J G_e \underline{u}_J \underline{u}_J^+ + \underline{\underline{I}} \qquad (3)$$

where G_e is the element gain, R_j is the interference power level of the $j\underline{th}$ source (relative to thermal noise referred to the element input) incident on the array aperture, $E \{ \cdot \}$ denotes the statistical expected value over the interference noise processes and $\underline{I}$ is the identity matrix. The N-1 degrees of freedom of the array are characterized by the N eigenvalues, $s_1, \ldots, s_N$, of the N x N matrix $\underline{\underline{R}}_A$. For J sources, J of the N eigenvalues of $\underline{\underline{R}}_A$ will be greater than unity, while the remaining N-J will be 1. However, if several of the interference sources are not orthogonal, i.e., they are in close proximity (relative to the array half-power beamwidth, HPBW), then not all of the s_1, ..., s_J will be significantly greater than 1. Otherwise said, the array in this case is not using a single degree of freedom per interference source present in order to accomplish the nulling. If the sources are orthogonal as defined in (2), however, all of the $s_1, \ldots, s_J$ must be significant, and in fact this condition leads to eigenvalues $s_1 = R_1, \ldots, s_J = R_J$. Equation (2) defines the conditions for orthogonal sources, and the presence of N-1 such sources necessarily uses up all of the available N-1 degrees of freedom of the array. (We note that if the array element spacing is so large that grating lobes appear over the FOV, then the number of possible positions for the $\underline{u}_j$ to satisfy Eq. (2) is multiplied.)

The concept of orthogonal sources can be quite useful in characterizing the performance of an array when operating over a wide bandwidth. Consider the presence of J orthogonal sources operating over a fractional bandwidth FBW. The correlation matrix for incoherent white noise sources is then given by

8

$$\underline{\underline{R}}_A = G_e \ R_1 \ < \underline{u}_1 \ \underline{u}_1^+ > + \ \ldots \ + G_e \ R_J \ < \underline{u}_j \ \underline{u}_j^+ > + \underline{\underline{I}} \tag{4}$$

where the bracket $< \cdot >$ denotes the integral

$$< \cdot > = \frac{1}{FBW} \int_{1-FBW/2}^{1+FBW/2} (\cdot) \ dw \tag{5}$$

and $w = \omega/\omega_0$ denotes the normalized frequency. Because of this frequency average, J sources now lead to the presence of an additional group of eigenvalues s_{J+1}, s_{J+2}, $\ldots \ s_{J+L}$ which arise due to bandwidth (see Ref. 6 for a more detailed discussion of this phenomenon). If FBW is large, the s_{J+1}, $\ldots \ s_{J+L}$ become significant and forming a wideband null on the sources uses up additional array degrees of freedom. This has two possible effects: if $J+L < N$, then the array will form broadband nulls, but these will also tend to be spatially broader than narrowband nulls and so will yield reduced antenna gain to the desired users in close proximity to the interference sources; if $J+L > N$, the array cannot null all the sources. Both effects are to be avoided, if possible, as they result in non-optimum array performance. The case $J+L < N$ is difficult to evaluate quantitatively, since the resulting loss in gain to a user signal which is tolerable is dependent on the system link margin parameters and the locations of the user and interference sources. However, if we consider the scenario consisting of N-1 equal, orthogonal interference sources, then $s_{N-1} >> s_N$ and the resultant eigenvalue s_N is directly indicative of the array bandwidth characteristics. Hence direct examination of s_N, treated as a function of FBW, offers a measure of the nulling bandwidth potential of a particular antenna configuration.

B.   The Tapped Delay Line and the Applebaum-Howells Processor

Fig. 2 illustrates the general topology of a tapped delay line, employing N_t taps/element, used in conjunction with an Applebaum-Howells type adaptive

9

k th ARRAY ELEMENT

$E_k(w)$

$\overline{n_0^2}$

TO SUM ← $\dot{A}_{k,1}$

⊕ ← $\dot{V}_{k,1}$

WEIGHT CONTROL

$e^{j\phi_0 w}$ = PHASE DELAY
BETWEEN TAPS

TO SUM ← $\dot{A}_{k,2}$

⊕ ← $\dot{V}_{k,2}$

WEIGHT CONTROL

TAPPED DELAY
LINE — N_t TAPS

TO SUM ← $\dot{A}_{k,N_t}$

⊕ ← $\dot{V}_{k,N_t}$

WEIGHT CONTROL
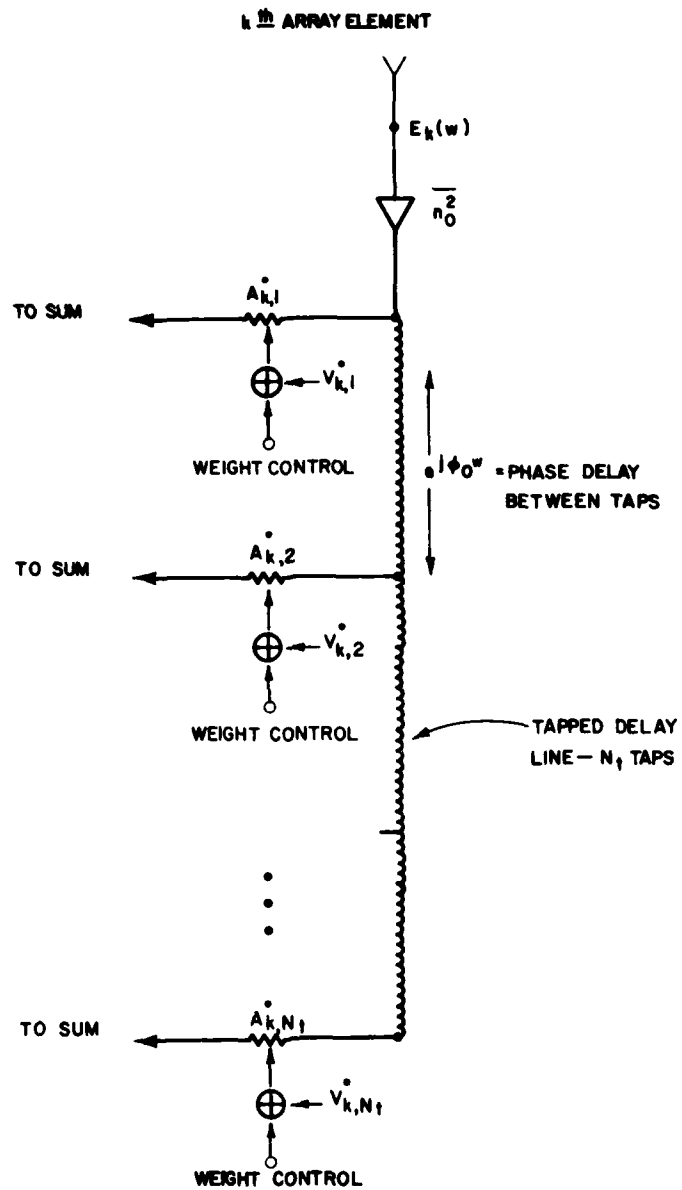
Fig. 2.   Topology of tapped delay line weighting scheme
illustrated for the kth element of an N-element array, and using
and Applebaum-Howells type adaptive processor.

10

processor. For simplicity only the schematic pertaining to the $k\underline{^{th}}$ element is shown in the figure. We use the following notation: the subscript "k" denotes the array element under consideration and the subscript "n" the location along the delay line. ϕ_0 denotes the tap spacing in degrees - i.e., $\phi_0 = \omega_0 T$, where T is the time delay between taps. The frequency response of the $k\underline{^{th}}$ array element is denoted as $E_k(w)$ and the frequency response of the output of the $n\underline{^{th}}$ tap in the $k\underline{^{th}}$ channel as $E_{k,n}(w)$. Since considerable loss may be encountered in the power division to the N_t taps, it is desirable to amplify before the delay line input. This is indicated in Fig. 2, depicting an amplifier at the output of each array element having thermal noise n_0^2. As a consequence of amplifying before the power split, the resultant thermal noise at the output of each tap in a given channel is correlated, as contrasted to the more familiar situation, without frequency compensation, in which the thermal noise is uncorrelated between channels. Because of this noise correlation effect, and because the algorithm chosen is one that tends to minimize received power, it is possible for the adaptive array to "turn itself off" if adequate constraints are not imposed on the weight control algorithm. For the Applebaum-Howells algorithm, these constraints are imposed via the beam-steering voltage $\underline{V}$, indicated in Fig. 2, which controls the weight in the absence of interference sources -- i.e., $\underline{V}$ specifies the quiescent radiation pattern of the array. The proper choice of $\underline{V}$ will be developed in the next sections, and will be seen to have a substantial effect on the nulling performance.

The outputs of each of the $N \cdot N_t$ terminals of the array define an $N \cdot N_t$ x $N \cdot N_t$ correlation matrix $\underline{\underline{R}}$ which governs the performance of the array. Once $\underline{\underline{R}}$ is determined, the weights can be set according to the chosen adaptive algorithm[5].

$$\underline{A} = [\underline{\underline{I}} + \mu\underline{\underline{R}}]^{-1} \cdot \underline{V} \tag{6}$$

where μ is the effective processor gain. μ is a variable, dependent on hardware considerations, and significantly affects the processor performance. Implicit in Eq. (6) is the assumption that $N \cdot N_t$ beam steering voltages

characterized by the vector $\underline{V}$ are applied to each weight at the output of each tap, and that $N \cdot N_t$ adaptively controllable complex weights are used. To develop the expression for $\underset{=}{R}$, consider the output of the nth tap behind the kth element:

$$E_{k,n} (w) = \frac{1}{\sqrt{N_t}} E_k(w) \, e^{-j(n-1)\phi_0 w} \tag{7}$$

where $E_k(w)$ is the array element output response. The contribution to $E_{k,n}(w)$ from thermal noise results in a noise covariance matrix given by

$$\underset{=N}{R} = \delta_{k,q} \frac{\overline{n_0^2}}{N_t} < e^{-j(n-m)\phi_0 w} > \tag{8}$$

The overall correlation matrix $\underset{=}{R}$ can be written as

$$\underset{=}{R} = \frac{1}{N_t} < E \{ E_k(w) \, E_q^*(w) \, e^{-j(n-m)\phi_0 w} \} > + \underset{=n}{R} \tag{9}$$

For J uncorrelated white-noise interference sources, and for an array antenna configuration, this expression for $\underset{=}{R}$ reduces to

$$\underset{=}{R} = \sum_{j=1}^{J} \underset{=j}{R} + \underset{=n}{R} \tag{10}$$

where

$$\underset{=j}{R} (k,q,n,m) = \frac{R_j \, G_e}{N_t} \cdot \frac{1}{FBW} \int_{1-FBW/2}^{1+FBW/2} e^{+j(\gamma_{k,j} - \gamma_{q,j})w} \, e^{-j(n-m)\phi_0 w} \, dw \tag{11}$$

12

where $q_{k,j} \equiv \dfrac{k_0 D}{2} \sin\theta_j (x_k \cos\phi_j + y_k \sin\phi_j)$ denotes the center frequency phase shift at the kth element due to the jth source. If R_j is normalized relative to n_0^2, then the resultant expression for $\underline{R}$ can be written as

$$\underline{R}(k,q,n,m) = \sum_{j=1}^{J} \underline{R}_j(k,q,n,m) + \frac{1}{N_t} \delta_{k,q} < e^{-j(n-m)\phi_0 w} > \tag{12}$$

This general expression for $\underline{R}$ will be used throughout the text to develop the specific properties of the adaptive array with delay line processing.

A careful examination of the expression for $\underline{R}$ in Eq. (12) and the adapted solution for the weights, Eq. (6), will indicate several parameters affecting the adaptive array performance. The most obvious are the tap spacing and number of taps per element. In order to simplify a tradeoff study characterizing the "optimum" tap spacing, we have assumed a uniform spacing between taps. Clearly for some scenarios, this is a non-optimum choice. For example, for a 3-element array with two sources incident at specified angles of incidence it can be shown that non-uniform tap-spacing gives the best performance (see Section IV). However, it might be argued that a fixed set of delay lines must be designed to handle arbitrary angles of incidence over the antenna FOV, in which case some angles of incidence necessarily yield better cancellation performance than others. Thus, optimum performance should be defined relative to, perhaps, the average cancellation performance over this range of angles. In this case, it would appear that the assumption of uniform spacing between taps is not so restrictive.

The algorithm defined by Eq. (6) defining the adapted weights is power level dependent as a consequence of the effective processor gain μ. Define $\underline{e}_i$ and s_i to be the eigenvectors and eigenvalues of $\underline{R}$, respectively. Then Eq. (6) can be expressed in the form

$$\underline{A} = \sum_{i=1}^{N \cdot N_t} \frac{1}{1+\mu s_i} (\underline{e}_i^{\dagger} \cdot \underline{V}) \, \underline{e}_i \tag{13}$$

Eq. (13) specifying the adapted weight vector $\underline{A}$ is similar in form to that for the more conventional Applebaum-Howells processor without tapped delay lines. Note that because of the term $1/(1+\mu s_i)$, the eigenvectors corresponding to the smaller eigenvalues are weighted more heavily, and must contain the information required to null the interference sources. The detailed characteristics of these eigenvectors corresponding to the lower eigenvalues will be developed in the next section. However, it is clear from Eq. (13) that the relative contribution of the eigenvectors corresponding to the smaller eigenvalues to the adapted solution for $\underline{A}$ is dependent on the processor loop gain μ; i.e., only eigenvalues s_i such that $\mu s_i \gtrsim 1$ are sensed by the processor. Define s_{MAX} to be the maximum eigenvalue of $\underline{\underline{R}}$. Then it can be shown that $s_{MAX} = N\, G_e\, R_j$ for a single source of relative power level R_j incident on the array. Consequently μs_{MAX} determines the dynamic range of incident power levels which will be sensed by the processor. Hence the performance of the delay line processor and the choice of "optimum" delay line parameters can be expected to be power level dependent. Only in the limit $\mu s_{MAX} >> 1$ can we determine optimum delay line parameters independent of incident power levels.

C. Optimum Weighting vs Delay Line Synthesized Weighting

In order to gain some insight as to how frequency compensation obtained using tapped delay lines improves the array performance, it is useful to define what we might refer to as an _optimum_ weight variation with frequency, and then examine how the frequency variation of the delay line synthesized weight compares to this optimum. As illustrated in Fig. 2, $E_k(w)$ denotes the frequency response transfer function of the $k\underline{th}$ antenna port, before delay line processing. Let us define the OPTIMUM weighting, $A_{0k}(w)$, k=1, ..., N, such that when $A_{0k}(w)$ is applied as weight to the $k\underline{th}$ antenna port output, then the interference sources are ideally nulled over the entire band defined by FBW. The output $V_0(w)$ as a function of w is given by

$$V_0(w) = \sum_{k=1}^{N} A_{0k}^{\ *}(w)\ E_k(w) \tag{14}$$

14

Noting Eq. (14), the optimum weights $A_{0k}(w)$ can readily be determined as follows: define the "narrowband" correlation matrix, $\underline{\underline{R}}_N(w)$, to be the N x N matrix at the array element outputs when J incoherent narrowband interference sources at frequency w are incident on the array, and w is considered a parameter over the interval $1 - FBW/2 \leq w \leq 1 + FBW/2$. Then $A_{0k}(w)$ are given by

$$\underline{A}_0(w) = [\underline{\underline{I}} + \mu\underline{\underline{R}}_N(w)]^{-1} \cdot \underline{V}_N \tag{15}$$

where $\underline{V}_N$ is an Nx1 equivalent steering vector. When considered as a function of w, $\underline{A}_0(w)$ minimizes the array output power over the entire nulling band defined by FBW. For comparison, consider the delay line synthesized weights obtained using N_t taps/element for an N-element array. From Fig. 2, the output voltage $V_0(w)$ is given by

$$V_0(w) = \sum_{k=1}^{N} \left\{ \sum_{n=1}^{N_t} A_{k,n}^* e^{-j(n-1)\phi_0 w} \right\} E_k(w) \tag{16}$$

The bracketed term in (16) corresponds to the frequency dependent weight synthesized by the delay line in the $k\underline{\text{th}}$ channel. We define, then,

$$A_k(w) = \sum_{n=1}^{N_t} A_{k,n} e^{+j(n-1)\phi_0 w} \tag{17}$$

to be this frequency dependent delay line synthesized weight. Eq. (17) defines a truncated Fourier series expansion for each weight $A_k(w)$ over the interval $1 - FBW/2 \leq w \leq 1 + FBW/2$. Ideally, $A_k(w)$ can be made to approximate $A_{0k}(w)$ as well as desired by choosing ϕ_0 appropriately and letting N_t be arbitrarily large. It is well known from the theory of such series expansions that in order to be able to approximate an arbitrary function over this band, $\phi_0 \leq 2\pi/FBW$. Note that if we choose $\phi_0 = 2\pi/FBW$, then $A_k(w)$ is periodic with period FBW. Consequently any Fourier sum approximating $A_{0k}(w)$ must exhibit the familiar Gibb's phenomenon ripple at the ends of the band, and leads to oscillating approximations to $A_{0k}(w)$ within the band. Typically the optimum weights

15

$A_{0k}(w)$ required depend only on the array dimensions (or array environment, if multipath arising from boundaries external to the array is present) and are generally slowly varying relative to $2\pi/FBW$. Consequently it is normally advantageous to choose $\phi_0 \leq 2\pi/FBW$. As long as $\phi_0 \leq 2\pi/FBW$, it is clear from the theory of Fourier series expansions that the approximation of $A_k(k)$ to $A_{0k}(w)$ will improve as the number of taps increases. It is the intention of the following sections to quantify this improvement with the objective of using only the minimum number of taps for a specified cancellation performance.

To obtain a feel for how well the delay-line synthesized weights defined by Eq. (17) approximate the ideal weights, $\underline{A}_0(w)$, consider an N-element array and a single interference source incident from an angle Θ,ϕ. Assume $\underline{V}_{-N}^{+} =$ [1, 0, ..., 0] corresponding to turning on only a single element (i.e., earth coverage for an array on a satellite). Choose the array phase reference relative to γ_1; then

$$A_{01}(w) = 1$$

$$A_{0k}(w) = -\frac{1}{N-1} e^{j(\gamma_k - \gamma_1)w}, \quad k=2, \ldots N \qquad (18)$$

By comparing Eqs. (17) and (18), several comments concerning the choice of ϕ_0 can be made:

1) Note that using N_t = two taps/element, no choice of ϕ_0 in Eq. (17) will yield exact synthesis of (18) unless N=2. In this case, for the two element array, let $\phi_0 = \gamma_2 - \gamma_1 = \Delta\gamma$; then the weighting $A_{1,2} = 0$, $A_{2,1} = 0$ results in perfect cancellation over FBW. If the angle of incidence defined by Θ,ϕ is allowed to be variable over the FOV, perfect cancellation of the interference waveform will be achieved only for selected angles of incidence for a fixed ϕ_0.

2) For N-elements, choosing N_t=N will not necessarily yield exact synthesis of the optimum weights using <u>uniform</u> tap spacing. Conversely, if a different tap-spacing $\phi_{0k} = \gamma_k - \gamma_1$ is used for each element, then a total of

$N_t = N$ taps are sufficient to perfectly cancel the interference over the band for selected angles of incidence.

3) Since any angle of incidence over the FOV is assumed equally probable, it is the average cancellation which can be achieved over this range of angles which becomes important. In this case, the use of uniform tap-spacing does not appear to be overly restrictive.

4) Referring to (17) and (18), an interesting graphical aid in visualizing how the choice of ϕ_0 affects the synthesis of the optimum weights can be developed. Consider a polar plot (amplitude/phase) of Eqs. (17) and (18), where for simplicity we consider only the case of 2 and 3 taps/element. Fig. 3a illustrates the graphical synthesis of the $A_{0k}(w)$ using 2 taps/element, and Fig. 3b using 3 taps/element. The optimum weight $A_{0k}(w)$ has a total phase traversal of $(\gamma_k - \gamma_1) \cdot$ FBW radians. For $A_{k,1}$ and $A_{k,2} \neq 0$, as would generally be the case for a fixed ϕ_0, then, at best, the vector sum of the delay line phasors can only approximate $A_{0k}(w)$. The two-element, two-tap special case, with $\phi_0 = \gamma_2 - \gamma_1$, becomes clear from Fig. 3a, in which case choosing $A_{k,1} = 0$ results in an exact synthesis of $A_{0k}(w)$. Fig. 3b for the three tap case illustrates the added degree of freedom obtained by adding the additional delay line. In both examples, ϕ_0 has been chosen too large, and the figures show the resultant too-rapid phase variation which would be obtained. This phase-amplitude plot will be used in the later sections to illustrate the performance of the delay line processor relative to optimum weighting for specific array antennas.
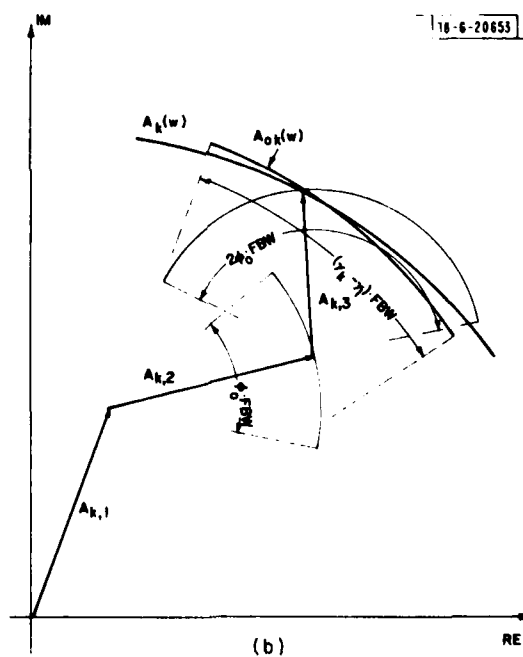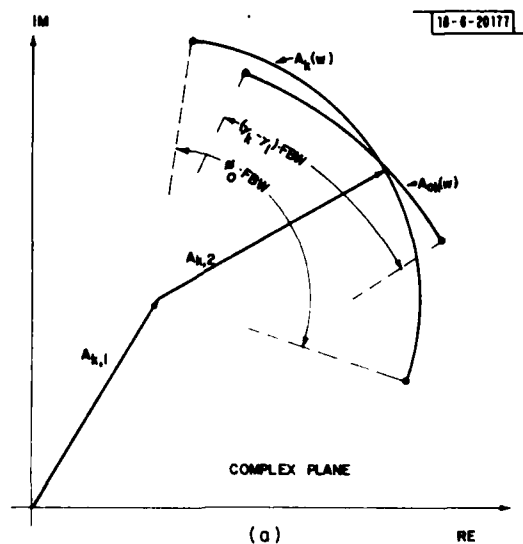
Fig. 3. Synthesis of the optimum weight $A_0(w)$ using tapped delay lines: (a) Amplitude/Phase plot using two taps/element, (b) Three taps/element.

18

III. THE TWO-ELEMENT ARRAY

The two-element array presents the simplest array antenna configuration which can be used to achieve radiation pattern nulling. Though simple in concept, a detailed analysis of its performance characteristics provides valuable insight into the mechanism of delay line frequency compensation. Practical considerations dictate that only the minimum number of taps required to achieve the desired array performance be used. With this goal in mind, the two-element, two-tap problem will be studied in some detail. For this simple case, analytical solutions for the delay line synthesized weights can be obtained together with analytical solutions for the optimum weights. In comparing the two solutions, it will become clear that exact synthesis of the optimum weights via two taps on a delay line is possible when the tap spacing is matched to the wavefront angle of arrival. However, for the practical case, this angle of arrival is not a priori known, so that this matched tap spacing could not be used. In practice, a fixed delay line spacing must be implemented to compensate for an arbitrary angle of arrival. For our purposes, we define an "optimum" delay-line tap spacing relative to this latter criterion. That is, the optimum delay-line tap spacing minimizes the average cancellation as a function of signal wavefronts incident from anywhere over the antenna FOV. Solutions for the optimum tap-spacing satisfying this criterion will be obtained for the two-element array for two taps on the delay line, and extrapolated to the N-element array employing a delay line with N_t taps via physical considerations. It is also possible to obtain analytical solutions for the eigenvectors and eigenvalues of the correlation matrix defined at the tap outputs for the two-element, two-tap array. Knowledge of these eigenvectors and eigenvalues allows a detailed examination of the adapted weights to be made on the basis of Eq. (13). In particular, the dependence of the array cancellation performance on processor dynamic range discussed in the previous sections can be developed. Finally, by extending the two-tap results to the more general $N_t > 2$, a quantitative assessment of the improvement in cancellation realized by increasing the number of taps can be made.

In the following, we first develop the characteristics of the eigenvalues and eigenvectors of $\underline{R}$ characterizing the performance of the two-element, two-tap topology, and examine each respective eigenvector in some detail. As might be expected, the eigenvector $\underline{e}_4$, corresponding to the lowest eigenvalue, contains the basic information on how to form nulls with delay line compensation. The transition of the adapted weight vector $\underline{A}$ defined in Eq. (13) to the optimum weighting defined by $\underline{e}_4$ is then considered as a function of processor dynamic range, μs_{MAX}. We show that as $\mu s_{MAX} \to \infty$, $\underline{A} \to \underline{e}_4$ to within a constant factor. Finally, given the case $\mu s_{MAX} \gg 1$, we determine the choice of ϕ_0 which maximizes the average interference cancellation for sources incident from anywhere over a fixed FOV.

A.   Eigenvectors and Eigenvalues of $\underline{R}$ for a Two-Tap Delay Line

Consider the two-element, two tap topology illustrated in Fig. 4. For convenience we define $E_0 = \sqrt{G_e R_j}$ and $\Delta\gamma = \gamma_1 - \gamma_2$. The solution is simplified considerably with little loss in generality if we ignore the effects of thermal noise. For a single interference source incident on the array, the 4 x 4 correlation matrix characterizing the delay line outputs is given by (see Eqs. 11 and 12)

$$\underline{R}_4 = (E_0^2)/2 < e^{+j(\gamma_k-\gamma_q)w} \, e^{-j(n-m)\phi_0 w} > . \qquad (19)$$

where we have defined $\gamma_{k,1} \equiv \gamma_k$ and $\gamma_{q,1} \equiv \gamma_q$. If the eigenvectors and eigenvalues of $\underline{R}_4$ can be determined, then using Eq. (13) the complete solution for the adapted weights, and other physically observable parameters, can be obtained. An exact analytical solution for these four eigenvalues and eigenvectors is difficult. However, they can be estimated quite accurately using a perturbation expansion of $\underline{R}_4$ on FBW.

To accomplish this, we expand the integrand of (19) about w=1. Define $\underline{R}_0$ according to

$$E_1 = E_0 e^{j\gamma_1 w} \qquad E_2 = E_0 e^{j\gamma_2 w}$$

$$\frac{E_0}{\sqrt{2}} e^{j\gamma_1 w} \qquad \qquad \frac{E_0}{\sqrt{2}} e^{j\gamma_2 w}$$

$$e^{-j\phi_0 w} \qquad \qquad e^{-j\phi_0 w}$$

$$\frac{E_0}{\sqrt{2}} e^{j(\gamma_1 - \phi_0)w} \qquad \frac{E_0}{\sqrt{2}} e^{j(\gamma_2 - \phi_0)w}$$
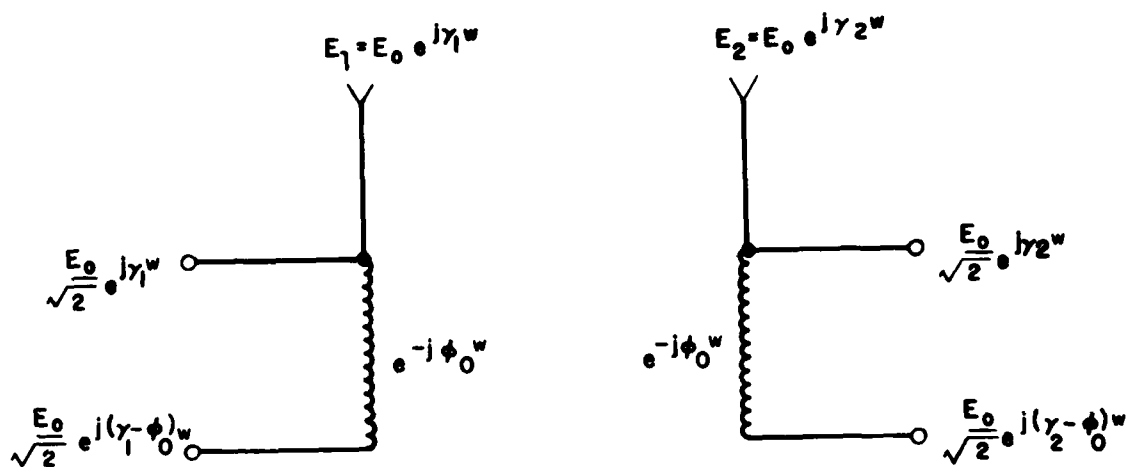
Fig. 4.   Delay line topology and notation for the two-element, two taps/element, delay compensated array.

$$\underline{\underline{R}}_0 \equiv \underline{\underline{R}}_4 \bigg|_{FBW=0} \qquad . \qquad (20)$$

Then $\underline{\underline{R}}_4$ can be written in the series expansion

$$\underline{\underline{R}}_4 = \underline{\underline{R}}_0 + \Delta\underline{\underline{R}}_2 + \Delta\underline{\underline{R}}_4 + \Delta\underline{\underline{R}}_6 \equiv \underline{\underline{R}}_0 + \Delta\underline{\underline{R}} \qquad , \qquad (21)$$

where $\Delta\underline{\underline{R}}_2$ is proportional to FBW^2, $\Delta\underline{\underline{R}}_4$ to FBW^4, and $\Delta\underline{\underline{R}}_6$ to FBW^6. (Note, odd powers of FBW are not present since $<\Delta w^n> = 0$ when n is odd, where $\Delta w = w - 1$.) The eigenvalues and eigenvectors of $\underline{\underline{R}}_4$ can be estimated by the expressions[7]

$$s_i = s_i^0 + \underline{e}_{i,0}^\dagger \cdot \underline{\underline{R}} \cdot \underline{e}_{i,0} \qquad (22a)$$

$$\qquad\qquad i = 1,2,3,4$$

$$\underline{e}_i = \underline{e}_{i,0} + \sum_{\substack{j=1 \\ j \neq i}}^{4} \frac{1}{s_i - s_{i,0}} \; (\underline{e}_{j,0}^\dagger \cdot \Delta\underline{\underline{R}} \cdot \underline{e}_{i,0}) \; \underline{e}_{j,0} \qquad (22b)$$

where the $s_{i,0}$ and $\underline{e}_{i,0}$, $i=1, \ldots, 4$ are the solutions to the unperturbed problem, (i.e., the eigenvectors and eigenvalues of $\underline{\underline{R}}_0$) and the s_i and $\underline{e}_i$, $i=1, \ldots, 4$ are the estimated eigenvalues and eigenvectors of $\underline{\underline{R}}$. Note by the form of $\Delta\underline{\underline{R}}$ that these estimates are correct to the order of FBW^6. The analysis leading up to the expression for the s_i and $\underline{e}_i$ is long and tedious. The procedure is outlined in Appendix B. The eigenvalues take the form

$$s_1 \simeq 2 \; E_0^2$$

$$s_2 \simeq E_0^2 \; (FBW \cdot \Delta\gamma)^2 \; (1 + \phi_0^2/\Delta\gamma^2)/24$$

$$(23)$$

$$s_3 \simeq 7.8 \times 10^{-4} \, E_0^2 \, (\phi_0^2/\Delta\gamma^2) \, (FBW \cdot \Delta\gamma)^4$$

$$s_4 \simeq 1.6 \times 10^{-6} \, E_0^2 \, (FBW \cdot \Delta\gamma)^6 \, (\phi_0^2/\Delta\gamma^2) \, (1 - \phi_0^2/\Delta\gamma^2)^2 / (1 + \phi_0^2/\Delta\gamma^2)$$

and the conjugate transpose of the normalized eigenvectors can be expressed as

$$\underline{e}_1^\dagger = \frac{1}{2} \left[1, \; e^{+j\Delta\gamma}, \; e^{j\phi_0}, \; e^{j(\phi_0+\Delta\gamma)} \right]$$

$$\underline{e}_2^\dagger = \frac{e^{-j\gamma_1}}{2\sqrt{1 + \phi_0^2/\Delta\gamma^2}} \left[(1 + \phi_0/\Delta\gamma), \; -(1 - \phi_0/\Delta\gamma) \, e^{+j\Delta\gamma}, \right.$$

$$\left. (1-\phi_0/\Delta\gamma)e^{+j\phi_0}, \; -(1+\phi_0/\Delta\gamma)e^{+j(\phi_0+\Delta\gamma)} \right]$$

$$\underline{e}_3^\dagger = \frac{1}{2} \left[-e^{-j\Delta\gamma}, \; 1, \; e^{-j(\Delta\gamma-\phi_0)}, \; -e^{+j\phi_0} \right] \tag{24}$$

$$\underline{e}_4^\dagger = \frac{1}{2\sqrt{1 + \phi_0^2/\Delta\gamma^2}} \left[(1 - \phi_0/\Delta\gamma)e^{-j\Delta\gamma}, \; (1 + \phi_0/\Delta\gamma), \; -(1 + \phi_0/\Delta\gamma) \cdot \right.$$

$$\left. e^{-j(\Delta\gamma-\phi_0)}, \; -(1 - \phi_0/\Delta\gamma)e^{+j\phi_0} \right]$$

Although Eqs. (23) and (24) are approximate, simulations have shown these expressions to be quite accurate for even the larger values of FBW near unity. One property of the eigenvalues is worth emphasizing. Since

$$\text{Trace} \; (\underline{\underline{R}}) = \text{Trace} \; (\underline{\underline{R}}_0) \quad , \tag{25}$$

and since $s_{20} = s_{30} = s_{40} = 0$, then it must follow that

23

$$s_{10} = s_1 + s_2 + s_3 + s_4 \qquad . \tag{26}$$

As FBW increases, since s_{10} is independent of FBW, generally s_1 begins to decrease and s_2, s_3 and s_4 increase so that (26) is satisfied. Hence since s_4 is the smallest, the approximation to s_4 in (23) is the most accurate.

We now show that, as contrasted to the eigenvalues of $\underline{\underline{R}}_A$ (where $\underline{\underline{R}}_A$ is the N x N correlation matrix defined at the <u>antenna</u> output ports), the eigenvalues of $\underline{\underline{R}}_4$ cannot be associated directly with output power relative to thermal noise. To see this, we note by definition that

$$s_i = \frac{\underline{e}_i^{\dagger} \cdot \underline{\underline{R}}_4 \cdot \underline{e}_i}{\underline{e}_i^{\dagger} \cdot \underline{e}_i} \qquad , \tag{27}$$

whereas the output power relative to thermal noise, $(I/N)_i$, when $\underline{e}_i^{\dagger}$ is applied as a weight is given by

$$(I/N)_i = \frac{\underline{e}_i^{\dagger} \cdot \underline{\underline{R}}_4 \cdot \underline{e}_i}{\langle \underline{A}^{\dagger}(w) \cdot \underline{A}(\underline{w}) \rangle} \qquad , \tag{28}$$

where $\underline{A}(w)$ is the delay line synthesized weight defined in Eq. (17). Thus $(I/N)_i$ is given by, using Eq. (8),

$$(I/N)_i = \frac{\underline{e}_i^{\dagger} \cdot \underline{\underline{R}}_4 \cdot \underline{e}_i}{\underline{e}_i^{\dagger} \cdot \underline{\underline{R}}_N \cdot \underline{e}_i} \qquad , \tag{29}$$

and $\underline{\underline{R}}_N$ is <u>not</u> a diagonal matrix. Consequently

$$(I/N)_i = s_i \, \frac{\underline{e}_i^{\dagger} \cdot \underline{e}_i}{\underline{e}_i^{\dagger} \cdot \underline{\underline{R}}_N \cdot \underline{e}_i} \qquad . \tag{30}$$

24

Hence although $(I/N)_i$ is proportional to s_i, a strict equality does not hold. Consequently, we interpret the s_i relative to output interference/thermal noise ratio in the loose sense indicated by Eq. (30).

B. Interpretation of the Eigenvectors and Eigenvalues

We have seen from Eq. (13) that the adapted weight vector which minimizes the array output power is comprised of a sum of eigenvectors, suitably weighted. It is instructive to examine the delay line synthesized weight and resultant output power when each eigenvector, $\underline{e}_i^{\dagger}$, i=1, ..., 4, in turn, is used as a weight vector. The results give some insight into the physical significance of the eigenvectors.

1. Tapped Output Weighted by $\underline{e}_1$ and $\underline{e}_2$

The first two eigenvalues, s_1 and s_2, can be interpreted similarly to the first two eigenvalues of the correlation matrix $\underline{\underline{R}}_A$ defined at the antenna element outputs. That is, we note that $s_1 \sim 2 E_0^2$ represents the maximum output power obtainable from the array. This output results from effective weights $A_1(w)$ and $A_2(w)$ which cause the two weighted channels to add in phase at the output. This results in a radiation pattern having a beam maximum pointed toward the interference, which is relatively independent of frequency. s_2 represents the familiar array dispersion phenomenon, which varies as FBW^2 compounded by dispersion introduced by the delay lines. It is zero for zero bandwidth and increases as the square of the bandwidth. Applying $\underline{e}_2^{\dagger}$ as a weight vector in essence puts a "zero-bandwidth" null on the source and generates a "monopulse" type radiation pattern. Examination of $A_1(w)$ and $A_2(w)$ using $\underline{e}_2^{\dagger}$ as a weight at the tap outputs shows that $A_1(w)$ and $A_2(w)$ are only <u>weakly</u> dependent on w. Consequently, weighting characterized by $\underline{e}_3^{\dagger}$ and $\underline{e}_4^{\dagger}$ represent the most interesting cases relative to broadband nulling. Furthermore, since s_1, $s_2 >> s_3$, s_4, it is only $\underline{e}_3$ and $\underline{e}_4$ which contributed significantly to the adapted weights. (Unless, of course, $\phi_0 \to 0$, in which case $\underline{e}_3^{\dagger} \cdot \underline{V}$ and $\underline{e}_4^{\dagger} \cdot \underline{V} \to 0$ in (13); the solution for $\underline{A}$ then reduces to that of frequency independent weighting at the array output for which s_2 characterizes the adapted array output power. This case is well understood.)

2. Tapped Output Weighted by $\underline{e}_3$

Using the expression for $\underline{e}_3^\dagger$ from Eq. (24) in Eq. (17) results in the delay line synthesized weights $A_1(w)$ and $A_2(w)$ given by:

$$A_1^*(w) = \frac{1}{2} e^{-j\Delta\gamma}[e^{-j\phi_0(w-1)} - 1] \tag{31a}$$

$$A_2^*(w) = \frac{1}{2}[1 - e^{-j\phi_0(w-1)}] \; . \tag{31b}$$

Equation (31) leads to an output voltage vs. frequency relationship, $V_0(w)$, given by

$$V(w) = A_1^*(w)\, E_1(w) + A_2^*(w)\, E_2(w)$$
$$= \frac{1}{2} e^{j\gamma_2}[e^{-j\phi_0(w-1)} - 1][e^{j\gamma_1(w-1)} - e^{j\gamma_2(w-1)}] \; . \tag{32}$$

Hence when $\underline{e}_3^\dagger$ is used as weight vector, the resultant output at $w=1$ is zero by virtue of the fact that each $A_k(w=1)=0$, i.e., __the array turns off__ at band center, as opposed to cancelling the weighted interference between channels. Thus it would be undesirable to use $\underline{e}_3$ to synthesize the weights since the user signals as well as the interference signals are nulled. In order to assure that the adapted solution, Eq. (17) employs $\underline{e}_3$ in the solution as little as possible, we choose $\underline{V}$ so that $\underline{V}^\dagger \cdot \underline{e}_3 = 0$ which from Eq. (13) prevents $\underline{e}_3$ from contributing to the adapted weight. This condition will be satisfied if we choose $\underline{V}$ of the form:

$$\underline{V}^\dagger \alpha \; [v_1^*, \; v_2^*, \; v_1^* \, e^{j\phi_0}, \; v_2^* \, e^{j\phi_0}] \; . \tag{33}$$

where v_1 and v_2 are arbitrary complex constants. Physically this choice of $\underline{V}$ corresponds to a quiescent weighting behind a specific element so that the ouputs of each tap add __in phase__ in the absence of interference.

26

For example, consider a wavefront normally incident on the array. Two possible choices of $\underline{V}^\dagger$ can be used to turn on array element number one, if an earth coverage quiescent radiation pattern is desired. One choice would be: $\underline{V}^\dagger = [1,0,0,0]$, which is inconsistent with Eq. (33) above. For this choice of $\underline{V}^\dagger$, an allowable adapted weight vector $\underline{A}$ which results in minimum output power would be $\underline{A}^\dagger = [1,0,-e^{j\phi_0}, 0]$. This adapted weight turns off the array at band center (i.e., $A_1(w=1)=0$ and $A_2(w=1)=0$). However, choosing $\underline{V}^\dagger$ of the form $\underline{V}^\dagger = [1,0, + e^{j\phi}0,0]$ prevents this situation from occurring, since $\underline{A}^\dagger$ can no longer contain a component of $\underline{e}_3$. The latter choice of $\underline{V}^\dagger$ assures $\underline{V}^\dagger \cdot \underline{e}_3 = 0$. Additionally, this choice of $\underline{V}$ gives maximum output of the delay lines in the quiescent mode of operation.

When $\underline{e}_3^\dagger$ is applied as a weight, s_3 governs the adapted output power of the array. Note the dependence $s_3 \propto \phi_0^2 \Delta\gamma^2 FBW^4$. As $\phi_0 \to 0$, then $s_3 \to 0$. Thus, for $\phi_0 = 0$, the only possible means of obtaining zero output power when $FBW \neq 0$ is for the array to turn itself off by adjusting the output of the taps (the delay line is only a simple power divider in this limiting case) to be 180° out of phase with each other.

3. Tapped Output Weighted by $\underline{e}_4$

Examination of the eigenvalue s_4 shows that it goes to zero when $\phi_0 = 0$ and $\phi_0 = \Delta\gamma$, independent of FBW. The case $s_4 = 0$ when $\phi_0 = 0$ is similar to the situation discussed above. It leads to the trivial solution of zero output power results from turning off the array. The case $s_4 = 0$ when $\phi_0 = \Delta\gamma$ leads to the desired optimum result. That is, applying $\underline{e}_4^\dagger$ as weight leads to the optimum $A_1(w)$ and $A_2(w)$ synthesized using two taps/element. These are given by

$$A_1^*(w) = \frac{e^{-j\Delta\gamma}}{2\sqrt{1 + \phi_0^2/\Delta\gamma^2}} \left[(1 - \phi_0/\Delta\gamma) - (1 + \phi_0/\Delta\gamma)e^{-j\phi_0(w-1)} \right]$$

$$(34)$$

$$A_2^*(w) = \frac{1}{2\sqrt{1 + \phi_0^2/\Delta\gamma^2}} \left[(1 + \phi_0/\Delta\gamma) - (1 - \phi_0/\Delta\gamma)e^{-j\phi_0(w-1)} \right]$$

27

Comparing $A_1(w)$ and $A_2(w)$ in Eq. (34) to the optimum $A_{01}(w)$ and $A_{02}(w)$ which null the interference sources over the entire band yields exact comparison when $\phi_0 = |\Delta\gamma|$. Note that since $\Delta\gamma = k_0 D \sin \Theta$, then the delay line synthesized weighting is <u>independent of the sign of Θ</u>. Hence when $\Delta\gamma > 0$ and $\phi_0 = \Delta\gamma$, Eq. (34) reduces to

$$A_1^*(w) = -\frac{1}{\sqrt{2}} e^{-j\Delta\gamma w}$$

$$A_2^*(w) = +\frac{1}{\sqrt{2}}$$

$$(35)$$

and when $\Delta\gamma < 0$ and $\phi_0 = |\Delta\gamma|$, we obtain

$$A_1^*(w) = \frac{1}{\sqrt{2}} e^{-j\Delta\gamma}$$

$$A_2^*(w) = -\frac{1}{\sqrt{2}} e^{-j\Delta\gamma} e^{+j\Delta\gamma w}$$

$$(36)$$

Substituting either (35) or (36) into Eq. (16) yields perfect cancellation of the interference sources over the entire band.

4.   Simulations

The approximations to the s_i and $\underline{e}_i$ defined in Eqs. (23) and (24) have been verified by computer simulation using the exact solution outlined in Section II for the N-element-N_t tap topology. Figure 5 illustrates the general variation of the eigenvalues as ϕ_0 is varied for parameter $\Delta\gamma \cdot FBW = 1.9$. Increasing $\Delta\gamma \cdot FBW$ leads to a much more pronounced resonance for the lowest eigenvalue s_4. Note that when $\phi_0 = |\Delta\gamma|$, the resultant output power $= 0$, as $s_4 = 0$ if $\underline{e}_4^+$ is applied as weights to the tapped delay line outputs. For $\phi_0 \gg |\Delta\gamma|$, $s_4 \propto FBW^6$ as predicted by Eq. (23).
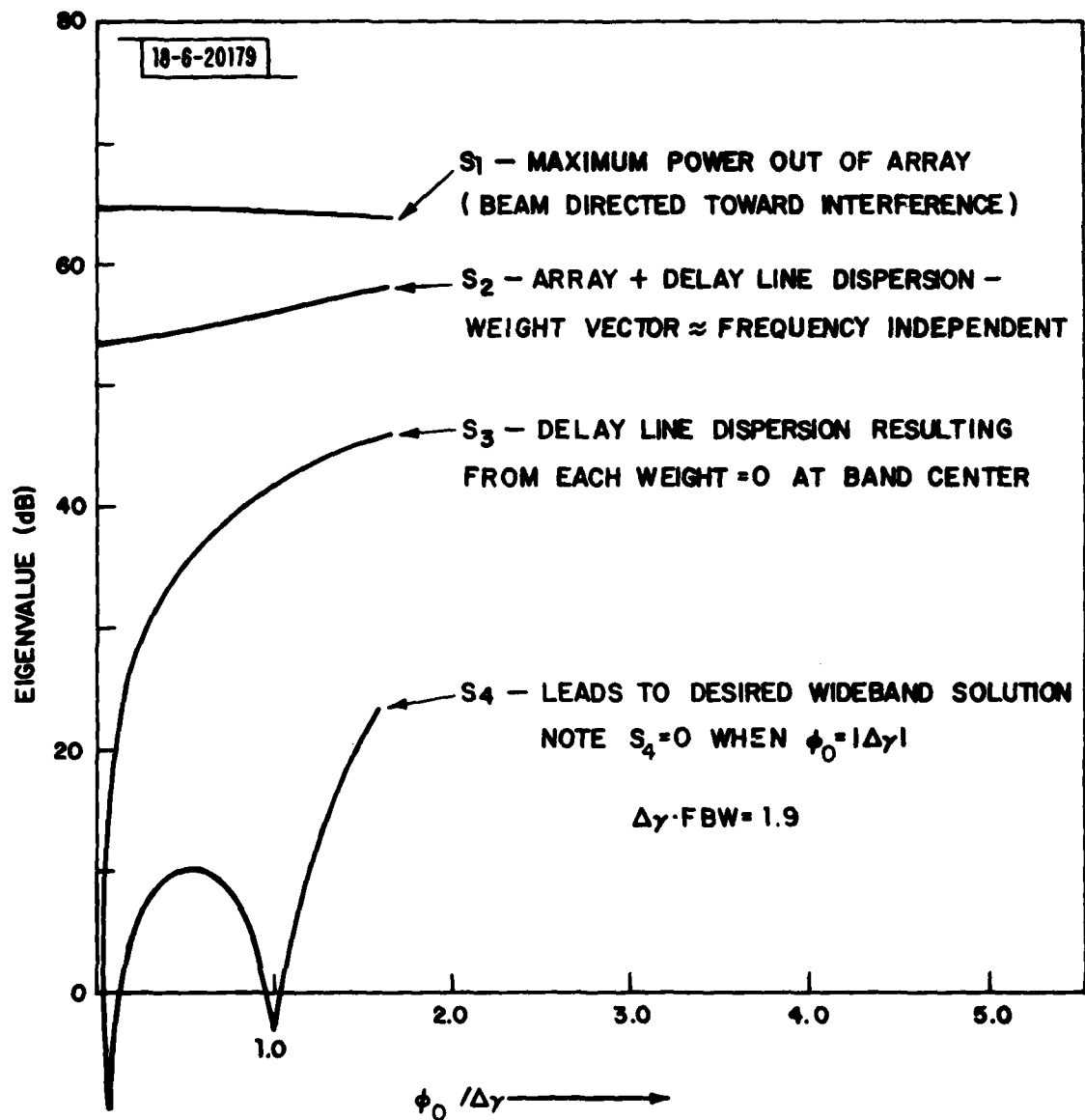
28

Fig. 5. Eigenvalue characterization vs tap spacing for the two-element array using two taps/element. $\Delta\gamma \cdot FBW = 1.9$.

C. Algorithm Dependence/Performance Evaluation

According to the above discussion, for a specified positioning of the interference source it is clear that optimum weighting results if $\phi_0 = |\Delta\gamma|$ and the eigenvector $\underline{e}_4{}^\dagger$ is applied as a weight to the tapped delay line outputs. However, in practice, the position of the interference source is not apriori known. Furthermore, it is desired that the weights be set autonomously according to some prescribed algorithm. Both of these factors dictate that perfect cancellation as governed by $\underline{e}_4$ for $\phi_0 = |\Delta\gamma|$ will not generally be achieved. For our purposes, we have chosen to fix the delay line phase ϕ_0 according to some prescribed value (to be determined later), and set the weights according to the Applebaum-Howells criterion specified by Eq. (6). Consequently the adapted weights are proportional to the sum of all the eigenvectors, each weighted according to $1/(1+\mu s_i)$. Generally $s_1 >> s_2$, s_3 and s_4, and we choose $\underline{V}$ according to Eq. (33), so that $\underline{e}_3{}^\dagger \cdot \underline{V} = 0$. Then the adapted weights take the form

$$A \approx \frac{1}{1 + \mu s_2} \ (\underline{e}_2{}^\dagger \cdot \underline{V}) \ \underline{e}_2 + \frac{1}{1 + \mu s_4} \ (\underline{e}_4{}^\dagger \cdot \underline{V}) \ \underline{e}_4 \quad . \tag{37}$$

The solution governed by Eq. (37) is broadband only when $\underline{e}_4$ dominates. For this to be true we require $\mu s_2 >> 1$ and ϕ_0 large enough so that $\underline{e}_4{}^\dagger \cdot \underline{V}$ is not small (note, from Eqs. (24) and (34), $|\underline{e}_4{}^\dagger \cdot \underline{V}|^2 \propto (\phi_0/\Delta\gamma)^2$, which approaches zero as $\phi_0 \to 0$). In turn, the degree to which μs_2 is much greater than unity depends on the loop gain μ (the value of which is more conveniently specified in terms of the processor dynamic range, μs_{MAX}), and on the bandwidth FBW. Consequently the performance of the delay line processor used in conjunction with an Applebaum-Howells power inversion algorithm can be expected to be a function of the variables μs_{MAX}, $\phi_0/\Delta\gamma$ and FBW. Since the eigenvalues themselves are a function of FBW by way of the parameter $\Delta\gamma \cdot$FBW, this latter parameter offers a more universal characterization of the results.

The above discussion illustrates that the cancellation C is a function of the three parameters μs_{MAX}, $\phi_0/\Delta\gamma$ and $\Delta\gamma \cdot$FBW, where C, defined as

$$C = \frac{(I/N)_a}{(I/N)_b} \tag{38}$$

is the ratio of the interference to thermal noise before and after nulling the interference sources. In Eq. (38), $(I/N)_b$ and $(I/N)_a$ are given by

$$(I/N)_b = \frac{\underline{V}^\dagger \cdot \underline{\underline{R}}_4 \cdot \underline{V}}{\underline{V}^\dagger \cdot \underline{\underline{R}}_N \cdot \underline{V}} \quad ; \quad (I/N)_a = \frac{\underline{A}^\dagger \cdot \underline{\underline{R}}_4 \cdot \underline{A}}{\underline{A}^\dagger \cdot \underline{\underline{R}}_N \cdot \underline{A}} \tag{39}$$

It is possible to then evaluate Eq. (38) analytically using Eq. (37) for $\underline{A}$. However, the result is tedious and will not be carried out here. Rather we illustrate in Figs. 6, 7 and 8 the dependence of C on these parameters as each is varied for fixed values of the remaining ones. The results were obtained from computer simulation, and are not dependent on the perturbation expansion technique.

Figs. 6a and b illustrate the dependence of C as $\phi_0/\Delta\gamma$ is varied for $\Delta\gamma \cdot FBW = 1.0$ and 4.0, respectively, with μs_{MAX} as a parameter. Note that, as predicted from the behavior of e_4, when $\Delta\gamma \cdot FBW$ is large, and $\mu s_{MAX} \gg 1$, a pronounced resonance in the dependence of C on $\phi_0/\Delta\gamma$, indicating broadband cancellation is achieved. The _width_ of the resonance is dependent on the values of $\Delta\gamma \cdot FBW$, as can be seen by comparing Figs. 6a and b. Note that for $\Delta\gamma \cdot FBW \leqslant 1$, the resonance is quite broad, indicating that employing two taps/element is adequate to give good cancellation over a wide range of interference-source-locations, with fixed tapped spacing. However, as the aperture dispersion increases (either by increasing FBW or $\frac{D}{\lambda} \sin \Theta$), _more than two taps/_ element would be required to achieve deep, broadband cancellation over a wide FOV.

Figs. 7 and 8 illustrate the same general behavior as Fig. 6, only presented using differing values of the three parameters. Fig. 7 illustrates the dependence of C vs $\phi_0/\Delta\gamma$ as the parameter $\Delta\gamma \cdot FBW$ changes, for a fixed power level μs_{MAX}, whereas Fig. 8 shows the dependence of C on μs_{MAX} with

31

Fig. 6. Cancellation (dB) vs tap spacing for the two-element, two tap array with μs_{MAX} and $\Delta\gamma \cdot$ FBW fixed: (a) $\Delta\gamma \cdot$ FBW = 1.0, (b) $\Delta\gamma \cdot$ FBW = 4.0.

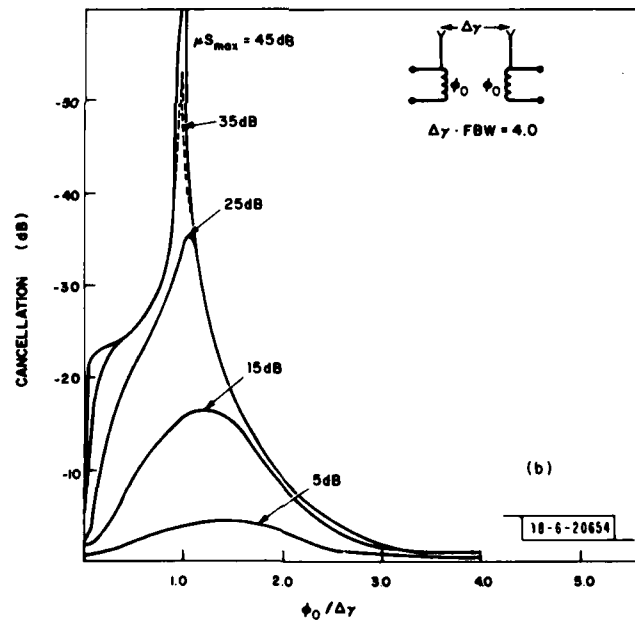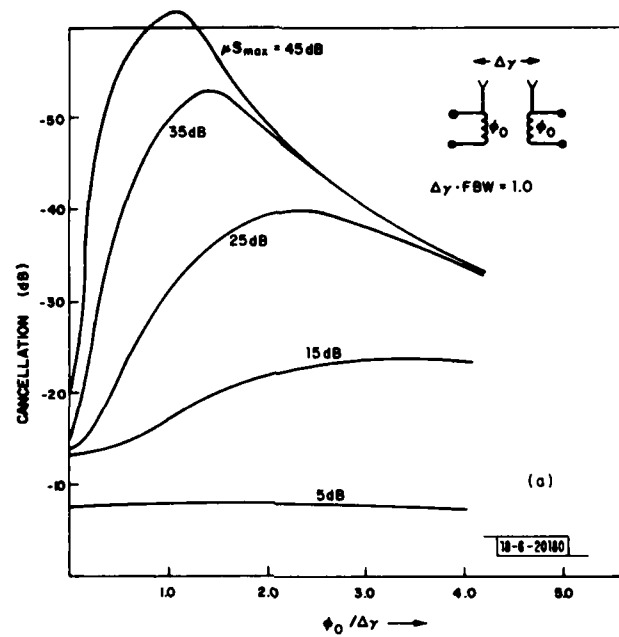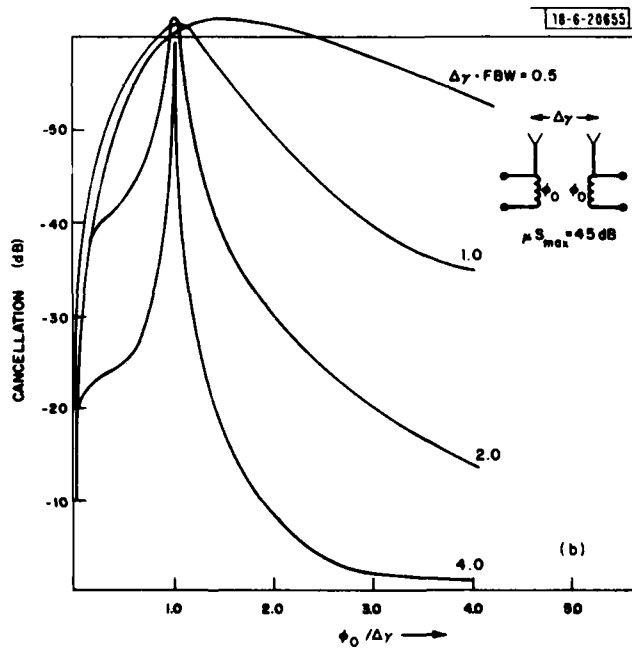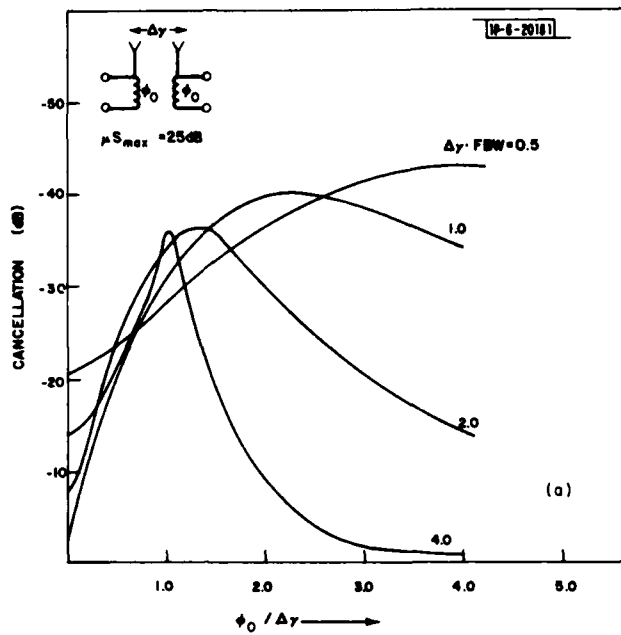Fig. 7. Cancellation (dB) vs tap spacing for the two-element, two tap array with μs_{MAX} and $\Delta\gamma \cdot FBW$ fixed: (a) $\mu s_{MAX} = 25$ dB, (b) $\mu s_{MAX} = 45$ dB.
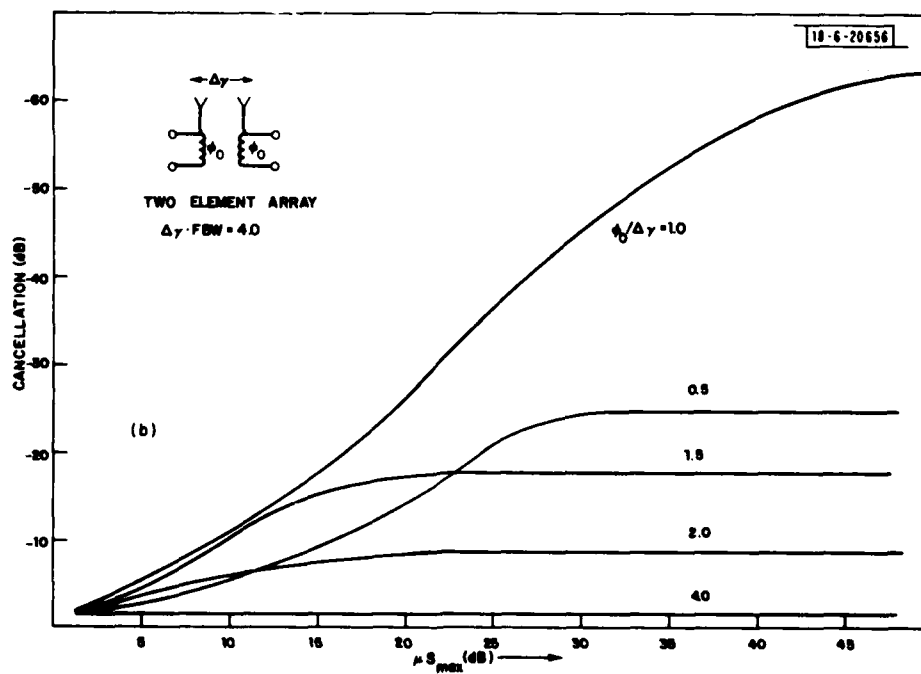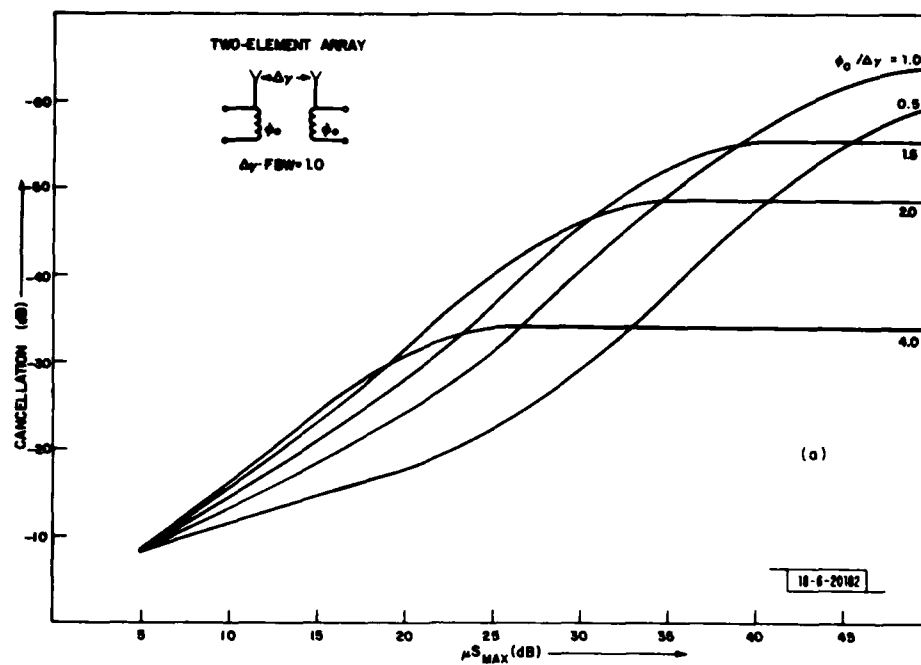
33

Fig. 8. Cancellation (dB) vs μs_{MAX} for the two-element, two tap array with $\Delta\gamma \cdot$ FBW and tap spacing fixed: (a) $\Delta\gamma \cdot$ FBW = 1.0, (b) $\Delta\gamma \cdot$ FBW = 4.0.

34

$\phi_0/\Delta\gamma$ as a parameter and $\Delta\gamma \cdot$ FBW fixed. Note from Fig. 8 that a limit exists where C becomes independent of power level. This limit is a fundamental limit based on the array and delay-line geometry, on the bandwidth, and on the interference source location. It could not be improved by use of another algorithm. In this region, one is in essence applying the eigenvector $\underline{e}_4^+$ as weights to the tap outputs. Fig. 8 illustrates that if the processor gain μ is set so that, for example, $\mu s_{MAX} \gtrsim 30\text{--}35$ dB, then 40 dB cancellation is possible on these larger sources over a broad range of $\phi_0/\Delta\gamma$, corresponding physically to a wide range of incidence angles. This indicates that, in general, a set of fixed delay line parameters exist where significant cancellation can be achieved compatible with a wide range of source scenarios. Optimization of this choice of delay line parameters for differing source scenarios is the objective of the following section.

D. Optimize ϕ_0 for a Predetermined FOV

The above results have indicated that if $\Delta\gamma$ were known (i.e., the incident angle of arrival), then choosing $\phi_0 = |\Delta\gamma|$ yields optimum wideband cancellation for the two element array, using two taps/element ($N_t > 2$ will be considered in the next section). Generally, however, the interference may be located anywhere over the antenna FOV and the angle of arrival is not _a priori_ known. Hence it is of interest to optimize the choice of ϕ_0 for best average cancellation over a range of $\Delta\gamma$, say $-\Delta\gamma_m \leqslant \Delta\gamma \leqslant \Delta\gamma_m$. Since C is a function of μs_{MAX} as well as $\Delta\gamma \cdot$ FBW and $\phi_0/\Delta\gamma$, optimization on ϕ_0 is generally complicated. However, in the limit $\mu s_{MAX} \gg 1$, then the adapted weight is approximately the eigenvector $\underline{e}_4$. In this case, substituting the expression for $\underline{e}_4$ into Eq. (28), the interference/thermal noise ratio after adaption can be shown to be

$$(I/N)_a = s_4 \frac{1 + \phi_0^2/\Delta\gamma^2}{\phi_0^2/\Delta\gamma^2} \quad , \tag{40}$$

35

where we have approximated $< \underline{A}^\dagger(w) \cdot \underline{A}(w) > \approx \underline{A}^\dagger \cdot \underline{A}$ evaluated at $w=1$, and s_4 is defined in Eq. (23). It is straightforward to average $(I/N)_a$ over $-\Delta\gamma_m \leqslant \Delta\gamma \leqslant \Delta\gamma_m$ and maximize this average with respect to ϕ_0. This result is given by

$$\phi_0 = 0.775\Delta\gamma_m \quad . \tag{41}$$

Hence best average cancellation assuming the interference sources located any-where in the range $-\Theta_m \leqslant \Theta \leqslant \Theta_m$ results from choosing $\phi_0 \sim$ three quarters of $\Delta\gamma_m$. Note since C is independent of the sign of $\Delta\gamma$, only a single delay line is required to provide cancellation over both positive and negatives values of Θ.

Fig. 9 illustrates the resultant cancellation vs Θ (expressed in terms of $\Delta\gamma/\Delta\gamma_m$) using one and two taps/element as the incidence angle is varied over the interval $-\Theta_m \leqslant \Theta \leqslant \Theta_m$. $\Delta\gamma \cdot$FBW is fixed at 6.0 and ϕ_0 is fixed at 0.775 $\Delta\gamma_m$. Only positive values of Θ are plotted since the results are symmetric about $\Theta=0$. The choice of ϕ_0 used for two taps/element results in the best average cancellation over the FOV. Worst case results occur when $\Theta=\Theta_m$. Since the optimization criterion leading to $\phi_0=0.775$ $\Delta\gamma_m$ was somewhat arbi-trary, one might consider increasing ϕ_0 and minimizing the peak cancellation over $-\Theta_m \leqslant \Theta \leqslant \Theta_m$. The resultant ϕ_0 would be greater than 0.775 Θ_m.

E.   Extensions to $N_t > 2$

Depending on the parameter $\Delta\gamma_m \cdot$FBW and the cancellation required for a particular system, using only two taps/element might not yield adequate cancel--lation. In this section we briefly consider using multiple taps/element for the two-element array. It will become clear later that the general trends and baseline parameters characterizing the two-element array are directly appli-cable to the N-element array.

Consider, then, the performance of the two element array when $A_1(w)$ and $A_2(w)$ are synthesized using N_t taps/element, and assume the tap spacing ϕ_0 between taps is uniform. It is clear from Fig. (3) that increasing N_t leads to a better approximation of $A_{0k}(w)$ by $A_k(w)$. Of course, if $\phi_0 = |\Delta\gamma|$,
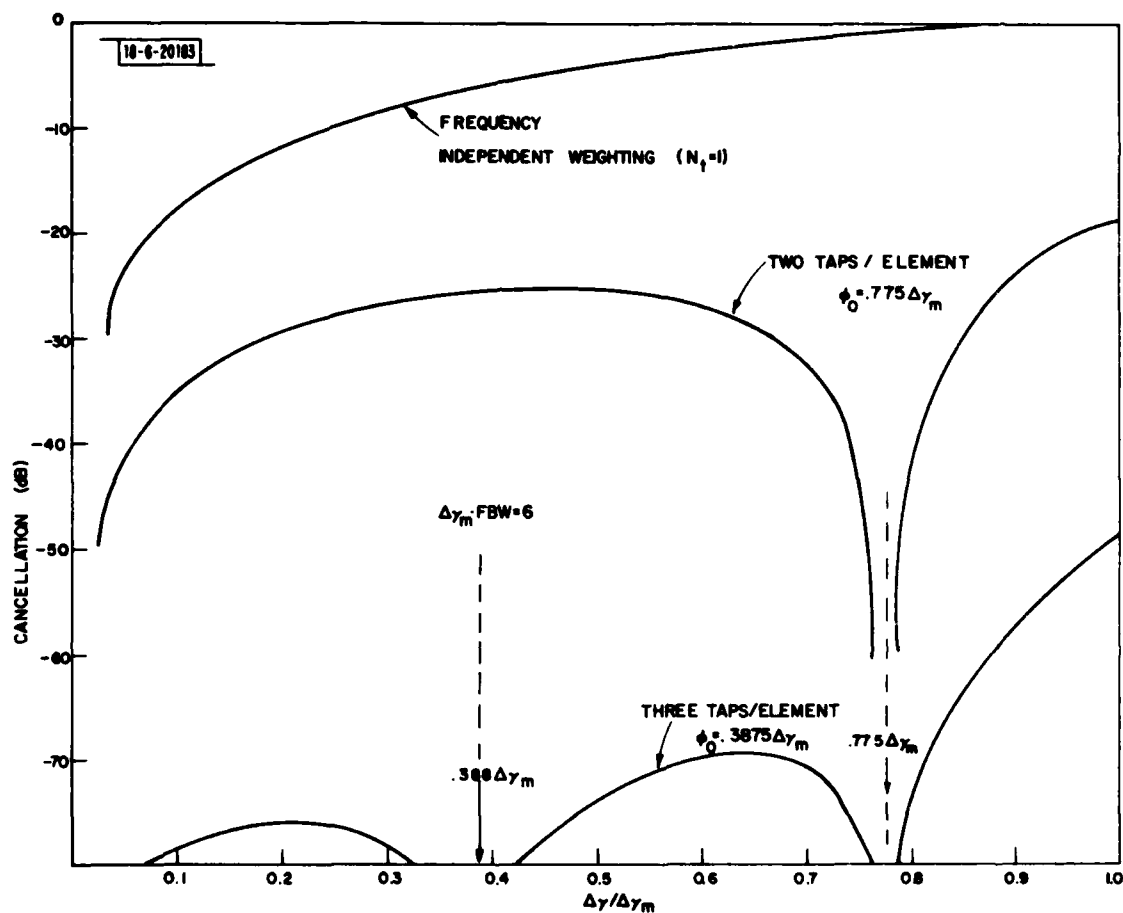
36

Fig. 9.   Cancellation (dB) vs angle of arrival for the two-element array using frequency independent weighting and delay line weighting with two and three taps per element.

there is no need for $N_t < 2$ as the optimim weights are synthesized exactly for this case. For this reason we fix the delay line spacing $\phi_0 < \Delta\gamma_m$ and vary Θ over the FOV as defined above. For $N_t=3$, we choose $\phi_0 = \frac{1}{2}(0.775 \, \Delta\gamma_m) = 0.3875 \, \Delta\gamma_m$ -- i.e., one half the optimum value of ϕ_0 for $N_t=2$. This approximates a nearly uniform separation in ϕ_0 when viewed as $\Delta\gamma$ varies over the field of view. This choice of ϕ_0 now yields perfect cancellation for <u>two</u> positive incidence angles: $\Theta = 0.775 \, \Theta_m$ and $\Theta = 0.3875 \, \Theta_m$. The cancellation realized using $N_t=3$ as Θ varies over the field of view is illustrated in Fig. 9 for comparison with the case $N_t=2$ discussed above. Note the marked improvement obtained. This improvement results from the additional freedom to cancel the interference source exactly at a second positive angle of arrival over the FOV, which reduces the average cancellation over the FOV considerably. Because of our choice of ϕ_0, worst case cancellation again occurs at $\Theta=\Theta_m$. Of course, by adjusting ϕ_0 appropriately the dispersion at $\Theta=\Theta_m$ can be reduced, at the cost of degraded performance towards the center of the FOV.

Noting that worst case cancellation for our choices of ϕ_0 occur when $\Theta=\Theta_m$, the cancellation obtained for this angle of arrival can be used to characterize quantitatively the cancellation dependence on the number of taps as $\Delta\gamma_m \cdot$FBW is varied. To this end, Fig. 10 illustrates cancellation as $\Delta\gamma_m \cdot$FBW is varied using $N_t=1$, 2 and 3 and the same choices for ϕ_0 as in Fig. 9 (note, the curves for 3 and 6 elements will be discussed later). To obtain the result illustrated for the two element array, the angle of arrival $\Theta=\Theta_m$ and aperture diameter D/λ is fixed, and FBW is varied accordingly. The utility of the parameter $2\pi \cdot \frac{D}{\lambda} \sin \Theta_m \cdot$FBW in characterizing the delay line performance becomes clear from the results shown in the figure. For example, assume the antenna/delay line processor is to be designed to achieve 30 dB cancellation for interference sources located anywhere over the FOV. The system requirements (i.e., signal-interference resolution required, system bandwidth, etc.) determine the value of $\Delta\gamma_m \cdot$FBW required to realize a given performance specification. Clearly if $\Delta\gamma_m \cdot$FBW $\lesssim 0.25$, then frequency independent weights would suffice to realize the desired cancellation. If $0.25 \lesssim \Delta\gamma_m \cdot$FBW < 4, then a delay line using two taps/element should be employed;
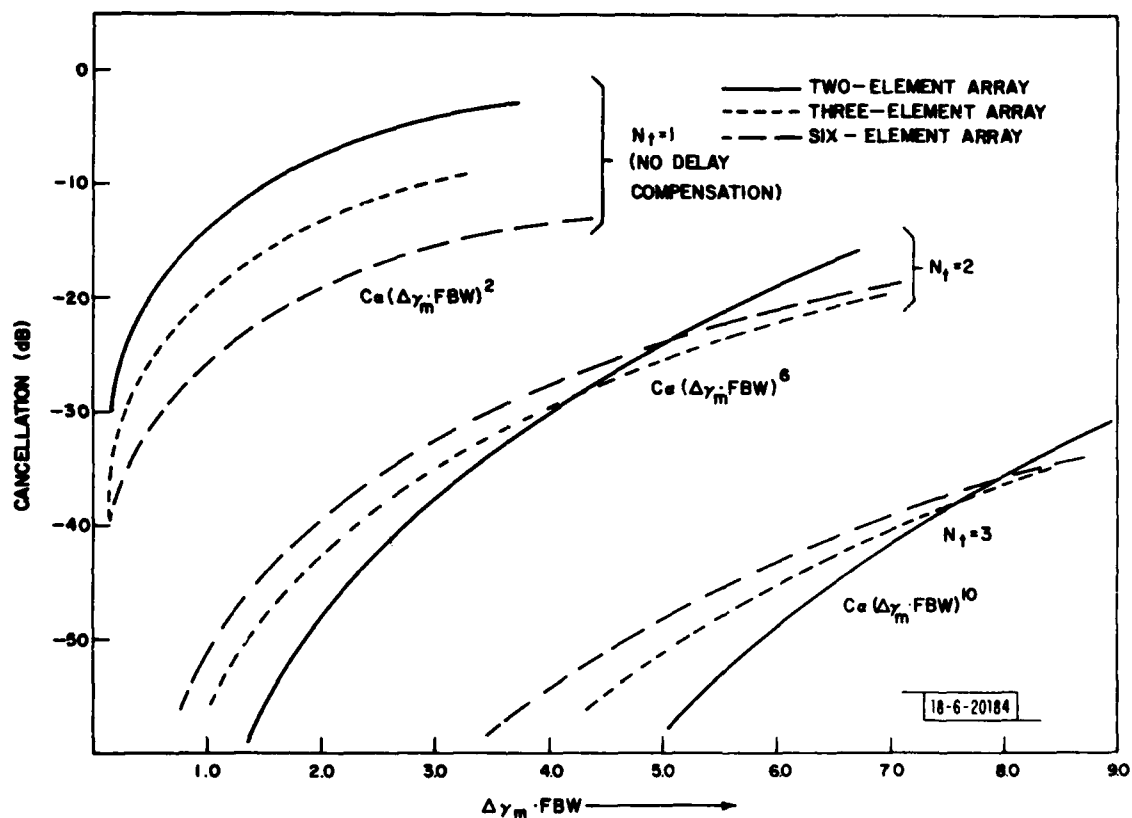
38

Fig. 10. Cancellation (dB) vs $\Delta\gamma \cdot$ FBW for the N-element linear array using N_t taps per element, where $\Delta\gamma \cdot$ FBW $= 2\pi \cdot \frac{D}{\lambda} \sin \Theta_m$ $\cdot$ FBW. N-1 orthogonal interference sources are equi-spaced beginning at $\Theta = \Theta_m$.

if $4 \leq \Delta\gamma_m \cdot FBW \leq 9$, three taps/element should be used, and so forth. The results for the three and six element arrays shown in Fig. 10 (to be considered later) indicate this characterization to be somewhat invariant to the number of elements.

One final observation can be made concerning the delay line performance results for $N_t > 2$; namely, the cancellation varies as a function of $(\Delta\gamma_m \cdot FBW)^\ell$, where ℓ is approximately given by $2(2N_t - 1)$. Thus for frequency independent weights $C \propto (\Delta\gamma_m \cdot FBW)^2$; for delay lines using two taps/element, $C \propto (\Delta\gamma_m \cdot FBW)^6$, and so forth for $N_t > 2$. This dependence can also be developed analytically using a bandwidth expansion for the correlation matrix similar to that used in Eq. (26). Generally, for N-1 sources, $\underline{\underline{R}}$ has $N \cdot N_t$ eigenvalues. The nulled output of the delay line processor is generally characterized by the smallest eigenvalue, $s_{N \cdot N_t}$, which it can be shown, for the two-element array varies according to $(\Delta\gamma_m^t \cdot FBW)^{2(2N_t - 1)}$, leading to the above-mentioned cancellation dependence. Knowledge of this variation with $\Delta\gamma_m \cdot FBW$ is often quite useful in scaling a known performance from one aperture size or bandwidth to another as a function of the number of taps.

IV. THE N-ELEMENT ARRAY

The results of the previous section yield quantitative estimates of the performance characteristics of a two-element array using either a 1, 2 or 3 tapped delay line for each element. When the number of array elements exceeds two, it is difficult to obtain analytical results, so that the majority of the analysis for $N > 2$ is based on numerical simulations. When N exceeds two, many configurations for array element positioning become possible, and it is intractable to consider all possibilities. For this reason, we concentrate our attention on the three classes of planar arrays illustrated in Fig. 11, each consisting of only a relatively small number of elements. For reasons which will become clear later, we classify the arrays according to their "angular dispersiveness", i.e., according to how spread out the N elements are relative to their angular distribution over a two dimensional planar aperture. For example, the simplest configuration having the least angular spread for N-elements distributed over a planar surface would be the equi-spaced linear array of elements illustrated in Fig. 11a. One might view such an array as consisting of two "radial arms" emanating from a common origin, on which the elements are positioned. The second configuration, having the next highest degree of angular spread has three radial arms, equi-spaced 120° in angular separation, on which the array elements are positioned. This class of arrays, which we refer to as triangular arrays, is illustrated in Fig. 11b. Finally, Fig. 11c illustrates four other array types, each characterized by greater than 3 radial arms emanating from a common origin, where the elements are positioned at the end-points of these arms. We classify these as "more complex arrays" relative to the triangular and linear arrays. Carrying through this delineation to N elements, $N \gg 1$, spread out uniformly over an aperture of fixed diameter, would lead to N radial arms, of varying radii, characterizing the planar array.
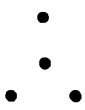
The basic idea behind this categorization of the array types considered is as follows: Eq. (15) defines the optimum weighting for an arbitrary N-element array. When the array elements are positioned according to simple geometrical

41
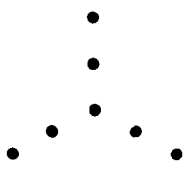
a)

SIMPLE TRIANGLE   SIMPLE DOUBLE TRIANGLE

b)

ROTATED DOUBLE TRIANGLE   HEXAGON

SQUARE   PENTAGON

c)

Fig. 11.   Three classes of planar arrays for use with delay line
compensation evaluation: (a) Equi-Spaced Linear Arrays, (b) Triangular
Arrays, (c) More complex arrays.

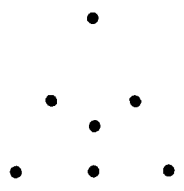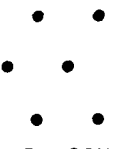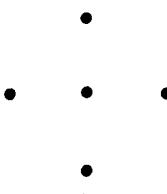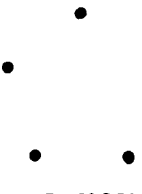relationships one would anticipate that the frequency variation of the optimum weights would be simply related between element outputs. (See, for example, Eq. (18) specifying $A_{0k}(w)$ for the N-element linear array.) Consequently, using a set of N_t taps equally spaced along a delay line would yield a better approximation to this simpler optimum frequency variation (when N_t is constrained to be small) than it would for the more complex frequency variation associated with the more complex arrays. Assuming this conjecture to be valid, one would then require fewer taps per element for an N-element linear array than for the more complex N-element arrays in order to achieve a desired cancellation performance. Otherwise said, the number of taps required depends more on the spatial complexity of the array rather than on the number of elements in the array. The following results offer support to the validity of this conjecture, although we can by no means present a definitive proof of its general applicability.

In the following, we consider first the simplest class of arrays -- the N-element linear array -- followed by the analysis for the triangular and more complex arrays.

A. The N-Element Linear Array

1. Three Elements: The three element linear array is an interesting extension of the two-element array because it allows for the presence of two interference sources located arbitrarily over the FOV, yet is still simple enough so that some analytical results can be obtained. One would anticipate that the amplitude and phase frequency variation of the optimum weights for the three element array becomes more complex when compared to that for the two-element array (for which the optimum weights have only phase variation), and hence a greater degree of synthesis capability is required to approximate this variation. Indeed, this turns out to be the case, but we shall see that the cancellation performance of the array still depends only weakly on the number of elements.

Consider the three-element, equi-spaced array illustrated in Fig. 12, and the two-source interference scenario defined by incidence angles Θ_1 and Θ_2.

18-6-20186

SOURCE 1

SOURCE 2

θ_2
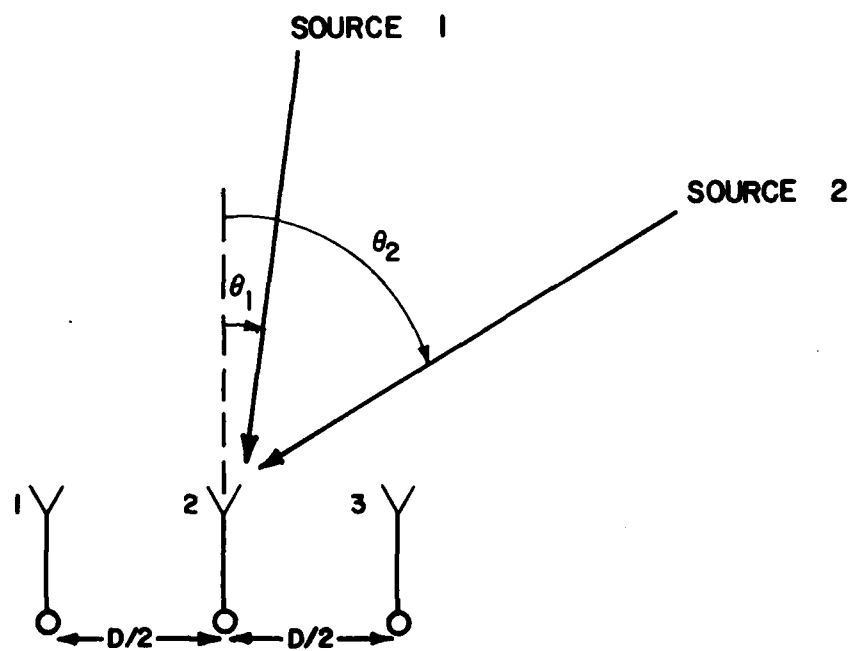
θ_1

1 2 3

← D/2 → ← D/2 →

Fig. 12. Geometry and notation for the three-element, equi-spaced linear array.

44

In keeping with notation introduced in Section III, define $\gamma_{k1} = \dfrac{k_0 D x_k}{2} \sin \Theta_1$ and $\gamma_{k,2} = k_0 D x_k/2 \sin \Theta_2$, k=1, 2, or 3, where the x_k are normalized element positions ($x_k^2 \leqslant 1$). If we choose $x_1 = -1$, $x_2 = 0$ and $x_3 = 1$ for element locations, then $\gamma_{2,1}$ and $\gamma_{2,2}$ reduce to 0, and $\gamma_{1,1} = -\gamma_{3,1}$, $\gamma_{2,1} = -\gamma_{3,2}$. This simplifies the analysis considerably. It is instructive to determine the optimum weight variation defined by Eq. (15) for this array, and use it as a basis for comparison to the tapped delay line synthesized weight. As before, denote these optimum weights as $A_{0k}(w)$, k = 1, 2, 3. Then it can be shown that

$$A_{01}(w) = A_{03}^{*}(w) = -e^{j\left(\dfrac{\gamma_{3,1} + \gamma_{3,2}}{2}\right) w}$$

(42)

$$A_{02}(w) = 2 \cos\left[\dfrac{(\gamma_{3,2} - \gamma_{3,1})}{2}\ w\right]$$

Observe that, as contrasted with the phase only variations of the optimum weighting for the two-element array, the $A_{0k}(w)$ in (42) have both amplitude and phase dependence on frequency. In fact, a careful examination of Eq. (42) reveals that it is not generally possible to synthesize $A_{0k}(w)$ exactly using a tapped delay line with a finite number of taps having equal tap-spacing. Consequently, the restriction of equal tap-spacing necessarily yields non-optimum results for some angles of arrival. However, due to its simplicity and practical utility, it is still a useful constraint to impose on the delay line design. Furthermore, it is certainly possible that when the array perfor-mance is averaged over all possible sets of incidence angles allowable over the FOV, uniform tap-spacing would still be the desired choice.

Consider now the synthesis of Eq. (42) using either one, two or three taps per element for the three-element array. Assume two orthogonal inter-ference sources located over the FOV, with one source positioned at maximum scan angle Θ_m. A second orthogonal source will be orthogonal to the first if it is positioned at Θ_2 satisfying the relationship

45

$$\frac{k_0 D}{2} (\sin \Theta_m \quad \sin \Theta_2) = 2\pi/3 \tag{43}$$

For small Θ_m (as for a satellite at geosynchronous altitude), we have $\Theta_m - \Theta_2$ ~ 2/3 λ/D. For the two sources so positioned, the resultant cancellation as $\Delta\gamma_m$ · BBW is varied (actually, to obtain the numerical results, we fix D/λ, Θ_1, Θ_2 and vary FBW) is plotted in Fig. 10, along with the results for the two element array*. For lack of a better criterion, we have chosen tap-spacing ϕ_0 according to the optimum spacing developed for the two-element array. This spacing tends to minimize the average cancellation when considered as a function of all angles of incidence over the FOV. Thus,

$$\phi_0 = .775 \ \Delta\gamma_m \ \text{for} \ N_t = 2$$

$$\tag{44}$$

$$\phi_0 = 3875 \ \Delta\gamma_m \ \text{for} \ N_t = 3$$

where $\Delta\gamma_m \equiv 2\pi \ D/\lambda \cdot \sin \Theta_m$. We have also chosen $\mu s_{MAX} >> 1$ so as to get at the fundamental nulling limitation of the array, independent of the algorithm implemented in the processor. Notice the close similarity between performance obtained for the two and three element array configurations as the number of taps is varied. In Figs. 13a, 13b and 13c, we examine the frequency dependence of the delay line synthesized weights $A_k(w)$ vs the optimum weights, $A_{0k}(w)$, of Eq. (42) using $\Delta\gamma_m \cdot$ FBW = 7.0. We utilize the polar representation of the weights introduced in Section II. Since each weight can be multiplied by an arbitrary complex function of frequency without changing the results, the results in Fig. 13 are normalized to $A_1(w)$ for each respective

---

*Note: These results, and all of the following simulations assume an earth coverage quiescent radiation pattern. Any other steering vector would increase or decrease the cancellation achieved by approximately the average quiescent gain to the interference sources relative to earth coverage gain.

In keeping with notation introduced in Section III, define $\gamma_{k1} = \dfrac{k_0 D x_k}{2} \sin \Theta_1$ and $\gamma_{k,2} = k_0 D x_k / 2 \sin \Theta_2$, k=1, 2, or 3, where the x_k are normalized element positions ($x_k^2 \leqslant 1$). If we choose $x_1 = -1$, $x_2 = 0$ and $x_3 = 1$ for element locations, then $\gamma_{2,1}$ and $\gamma_{2,2}$ reduce to 0, and $\gamma_{1,1} = -\gamma_{3,1}$, $\gamma_{2,1} = -\gamma_{3,2}$. This simplifies the analysis considerably. It is instructive to determine the optimum weight variation defined by Eq. (15) for this array, and use it as a basis for comparison to the tapped delay line synthesized weight. As before, denote these optimum weights as $A_{0k}(w)$, k = 1, 2, 3. Then it can be shown that

$$A_{01}(w) = A_{03}^{*}(w) = -e^{j\left(\dfrac{\gamma_{3,1} + \gamma_{3,2}}{2}\right)w}$$

(42)

$$A_{02}(w) = 2 \cos\left[\dfrac{(\gamma_{3,2} - \gamma_{3,1})}{2} w\right]$$

Observe that, as contrasted with the phase only variations of the optimum weighting for the two-element array, the $A_{0k}(w)$ in (42) have both amplitude and phase dependence on frequency. In fact, a careful examination of Eq. (42) reveals that it is not generally possible to synthesize $A_{0k}(w)$ exactly using a tapped delay line with a finite number of taps having _equal_ tap-spacing. Consequently, the restriction of equal tap-spacing necessarily yields non-optimum results for some angles of arrival. However, due to its simplicity and practical utility, it is still a useful constraint to impose on the delay line design. Furthermore, it is certainly possible that when the array performance is averaged over all possible sets of incidence angles allowable over the FOV, uniform tap-spacing would still be the desired choice.

Consider now the synthesis of Eq. (42) using either one, two or three taps per element for the three-element array. Assume two orthogonal interference sources located over the FOV, with one source positioned at maximum scan angle Θ_m. A second orthogonal source will be orthogonal to the first if it is positioned at Θ_2 satisfying the relationship

45

Fig. 13. Optimum weighting vs delay line synthesized weighting
for the three-element linear array: (a) Optimum weight variation
with frequency, (b) Delay line synthesized weight variation with
frequency using two taps/element.

47

DELAY LINE SYNTHESIZED
WEIGHTS USING THREE
TAPS / ELEMENT
$\phi_o = 0.3875 \, \Delta\gamma_m$

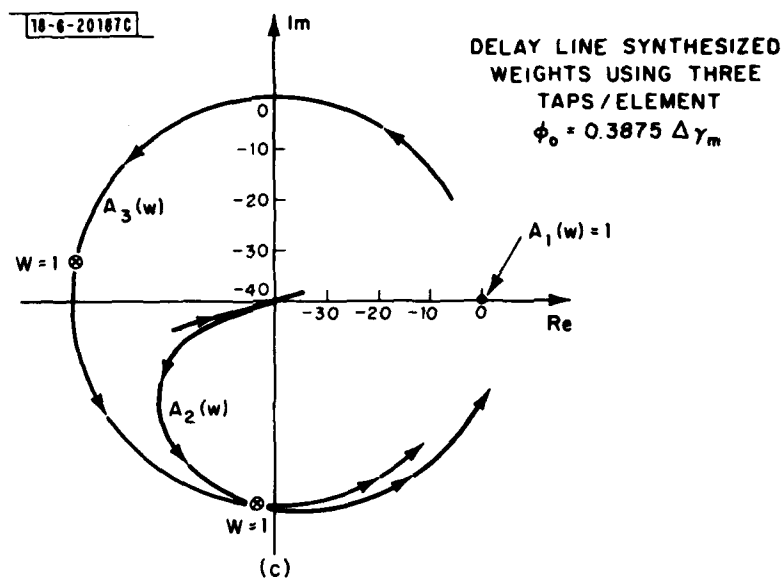$A_3(w)$

$A_1(w) = 1$

$W = 1$

$A_2(w)$

$W = 1$

(c)

Fig. 13 (Continued). Optimum weighting vs delay line synthesized weighting for the three-element linear array: (c) Three taps/element.

delay line case, and to $A_{01}(w)$ for the optimum weight variation. This allows for comparison on a one-one basis. Note, as obtained from Eq. (42), $A_{01}(w)$ and $A_{02}(w)$ illustrated in Fig. 13a are constant amplitude weights and $A_{03}(w)$ has a cosine variation with frequency with a peak amplitude of nearly 6 dB. The value of the $A_{0k}(w)$ at $w = 1$ is indicated in the figure. Figs. 13b and 13c illustrate the delay line synthesized approximation to the $A_{0k}(w)$ using 2 and 3 taps/element, respectively. At band center, $(w = 1)$, all the weights compare closely. As w increases from band center, the delay line synthesized weights begin to deviate from the optimum weights, although $A_2(w)$ and $A_3(w)$ have constant amplitude. The approximation to $A_{0k}(w)$ is worst at the edge of band, and it is here that the improvement realized in using 3 taps/element over 2 taps/element can be seen. This is particularly true of $A_3(w)$ for $N_t = 2$, where the approximation to $A_{03}(w)$ is very poor at the edge of the nulling band. For $N_t = 3$, $A_3(w)$ closely approximates $A_{03}(w)$. In order to illustrate how these deviations in $A_k(w)$ from $A_{0k}(w)$ affect the cancellation realized as a function of frequency, we illustrate in Figs. 14a and 14b the cancellation vs frequency over the nulling band obtained in the direction of each of the two sources. For $N_t = 1$, hardly any nulling results, whereas the improvement in cancellation realized in increasing N_t to either 2 or 3 is quite significant. Observe the cancellation is worst at the band edges consistent with the devia- tion of $A_k(w)$ from $A_{0k}(w)$ in these regions. The average cancellation over the nulling band can be obtained using Fig. 10 for $\Delta \gamma_m \cdot FBW = 7$, from which we obtain $C \sim -20$ dB using $N_t = 2$ and $C \sim -40$ dB using $N_t = 3$. Clearly these values are consistent with the cancellation vs frequency results illustrated in Fig. 14.

2.   The Six-Element Linear Array: In order to obtain a feel for the dependence of the number of taps on the number of elements, consider the six-element array illustrated in Fig. 11a. For this array, five orthogonally located interference sources can be positioned nearly uniformly over the FOV, similar to the positioning illustrated shown in the insert of Fig. 1. As before, we consider the cases $N_t = 1$, 2 or 3 using $\phi_0 = .775 \Delta \gamma_m$ for $N_t = 2$ and $\phi_0 = 0.3875 \Delta \gamma_m$ for $N_t = 3$. The resultant cancellation performance when
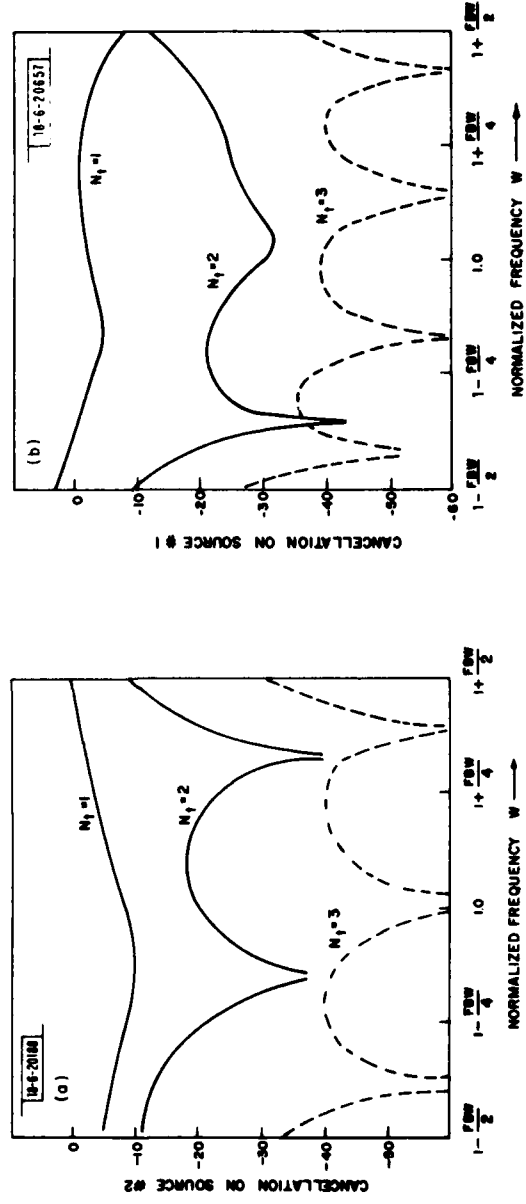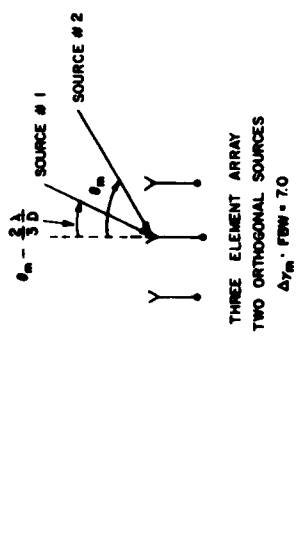
Fig. 14. Cancellation (dB) vs normalized frequency w for the three element linear array for $\Delta\gamma_m$. FBW = 7 as a function of the number of taps: (a) Cancellation in direction of source two, (b) Cancellation in direction of source one.

plotted vs $\Delta \gamma_m \cdot$FBW is illustrated in Fig. 10, for comparison with the two and three element array results. The general similarity of the results for all these arrays when $N_t = 2$ and $N_t = 3$ indicates that the performance achieved is only weakly dependent on the number of elements. Regions where one, two or three taps should be used to obtain a desired cancellation performance are readily identifiable. Note also the general applicability of the cancellation estimates obtained from the two-element array which predict $C \propto (\Delta \gamma_m \cdot \text{FBW})^2$ for $N_t = 1$, $C \propto (\Delta \gamma_m \cdot \text{FBW})^6$ for $N_t = 2$ and $C \propto (\Delta \gamma_m \cdot \text{FBW})^{10}$ for $N_t = 3$. Hence, we conclude that for the linear, equi-spaced array the key parameters governing the array performance are D/λ, $\sin \Theta_m$ and the fractional bandwidth. To first order these parameters can be used to estimate the number of taps required in order to achieve a desired wideband cancellation performance.

B. Triangular Arrays

The triangular arrays illustrated in Fig. 11b represent the simplest point of departure in considering the transition from linear arrays to planar arrays. In treating even simple planar arrays, the analysis becomes complicated due to the necessary inclusion of a two-dimensional FOV. However, the general concept of orthogonally positioned interference sources and their complete use of an array degree of freedom remains valid. Consequently, the general philosophy of positioning N-1 orthogonal (or nearly so) sources and examining the cancellation performance of the array relative to these sources as the nulling bandwidth increases can still be used to evaluate the array performance. Since aperture frequency dispersion is worse for sources located toward the edge of the FOV than for those near the center (see Fig. 1, cancellation without frequency compensation degrades as $(\Delta \gamma_m \cdot \text{FBW})^2$), we consistently position N-1 sources at these locations whenever possible. It should be emphasized, however, that when D/λ is large enough so that grating lobes occur over the FOV, the set of N-1 orthogonal source locations are not unique and cancellation performance is dependent on the set of source locations chosen. Consequently, locations chosen in the following analysis yield results which are only representative of the bandwidth characteristics of the array, and are not necessarily worst case.

With these restrictions in mind, consider the performance of the 4-element triangular array illustrated in Fig. 11b, subjected to three interference sources orthogonally located over the FOV. The cancellation vs $\Delta\gamma_m \cdot$FBW is illustrated in Fig. 15 for two different source location scenarios, illustrated in the insert in the figure, using values of $N_t = 1$, 2 and 3. The performance of the array vs the two scenarios is somewhat different for each case. However, even the poorest performance yields significant cancellation over the nulling band as the number of taps increases. Perhaps most significant is that using two taps per element yields only about 20-30 dB improvement over frequency independent weighting, whereas using 3 taps per element results in better than 50 dB (theoretical) improvement over that obtained using frequency independent weighting. Furthermore, the large cancellation levels realized tend to justify the choice of ϕ_0 used, which was extrapolated without justification from the two-element array analysis.

In order to investigate the dependence of cancellation on the number of elements, we fix the array symmetry (i.e., 3 radial arms specifying the element locations) and increase the number of elements from four to seven. The cancellation vs $\Delta\gamma_m \cdot$FBW for this array is illustrated in Fig. 16 for the 6-orthogonal source scenario indicated in the figure. Clearly, the cancellation realized as a function of $\Delta\gamma_m \cdot$FBW is not markedly different from that for the four-element triangular array, again indicating only a weak dependence of the delay line synthesis of $A_{0k}(w)$ on the number of elements. In fact, recognizing that the triangular array is comprised of three linear arrays rotated 120°, it should not be surprising that the results are not markedly different from the linear array. This supports the conjecture that the number of taps required in order to achieve very high cancellation levels is most strongly dependent on the angular dispersiveness of the array, i.e., N_t required is proportional to the number of radial arms characterizing the array.

C.   More Complex Arrays

Consider now the class of arrays illustrated in Fig. 11c, i.e., those requiring more than three angularly placed radial arms to specify their element

52
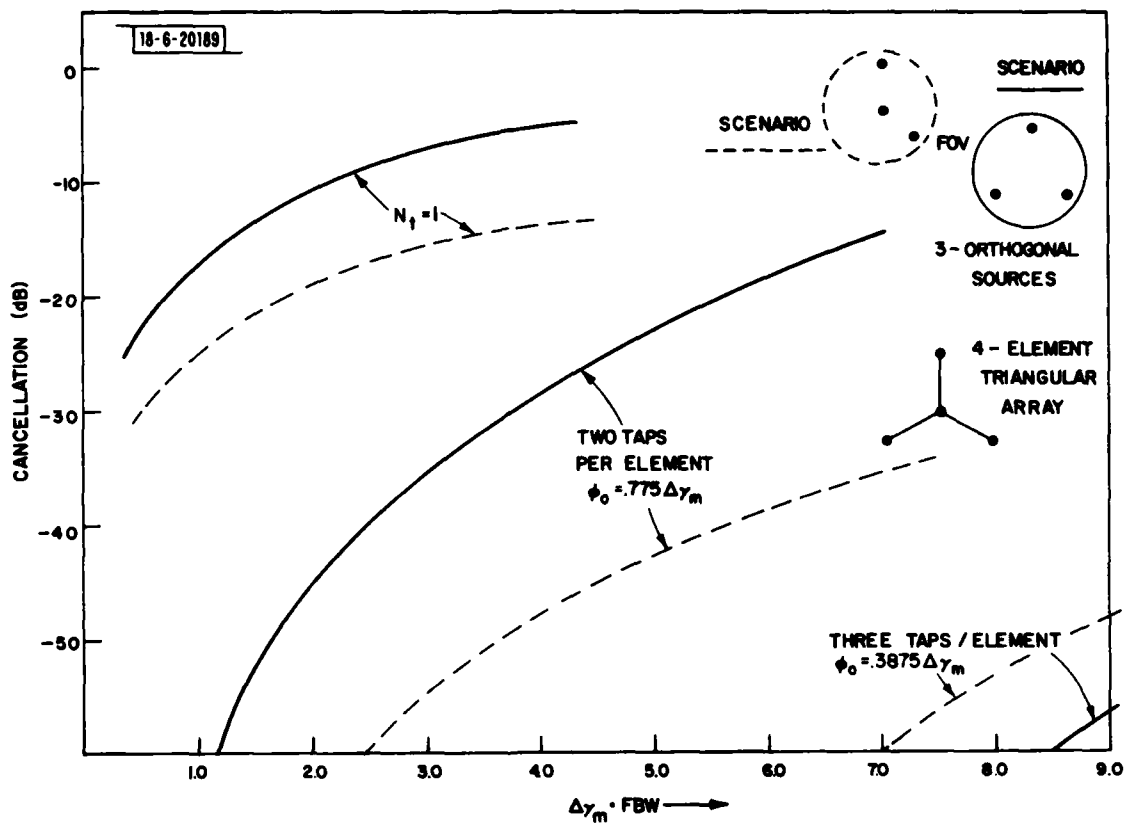
Fig. 15. Cancellation (dB) vs $\Delta\gamma_m \cdot$ FBW for the four-element triangular array using two different orthogonal, 3-source scenarios, as a function of the number of taps.
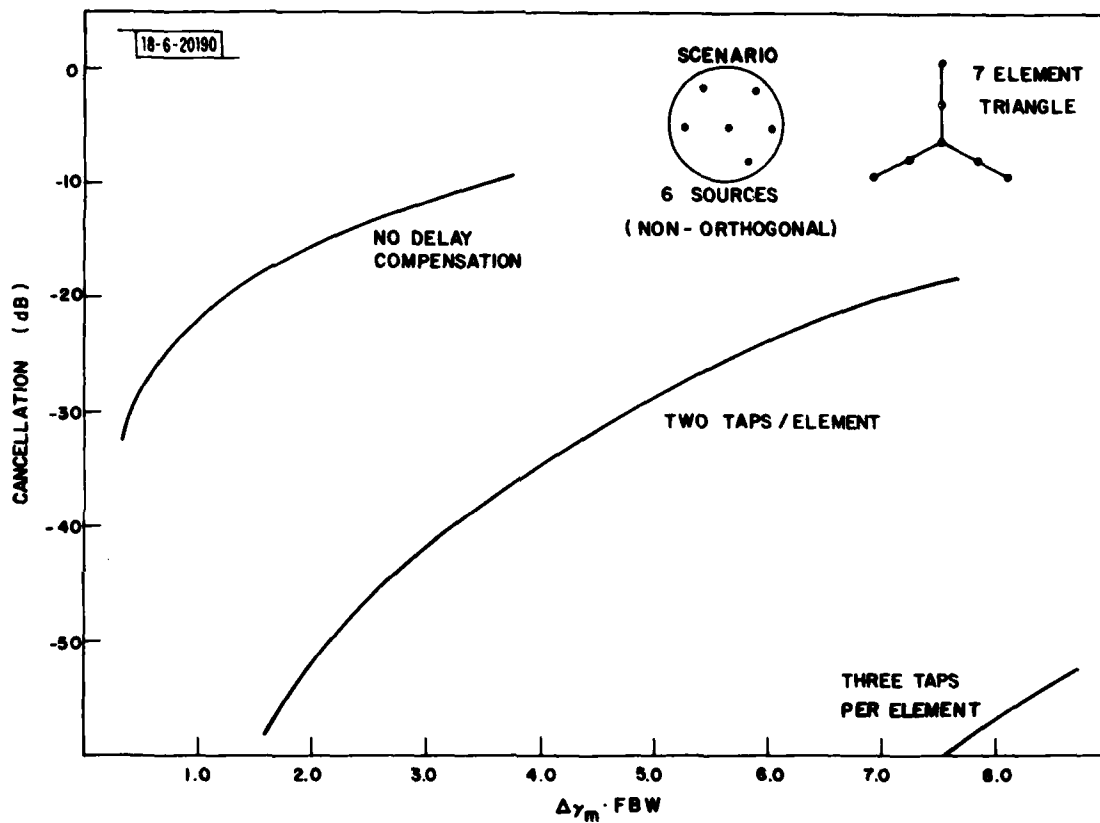
Fig. 16. Cancellation (dB) vs $\Delta\gamma_m \cdot$ FBW for the seven-element simple-triangular array using a six-source orthogonal scenario as a function of the number of taps.

locations. In order to illustrate the effect of radial element positioning on the cancellation performance, consider a simple modification to the 7-element triangular array treated above. If the inner triad of array elements of the 7-element triangular array of Fig. 11b is rotated 60°, the "rotated-double triangle" array illustrated in Fig. 11c results. This simple rotation of elements results in an array configuration characterized by 6 equi-spaced radial arms. The resultant cancellation vs $\Delta\gamma_m \cdot FBW$ performance relative to nulling a six-interference source scenario is illustrated in Fig. 17 using a one, two or three tapped delay line. The six-source scenario used to evaluate the array performance is a nearly-mutually orthogonal scenario (8 dB spread between the first six eigenvalues), chosen because a set of six mutually orthogonal sources for this array configuration does not appear to exist. Comparing Fig. 17 to Fig. 16, we conclude that the simple notational change from three to six radial elements drastically alters the array nulling band-width performance. This is because the more spatially dispersive the array, the more difficult it is for a fixed number of taps on a delay line to synthe-size the optimum weight variation with frequency. To see this, we illustrate in Figs. 18 and 19 the optimum synthesized tapped delay line weights variation with frequency for the scenario considered using the simple double triangle configuration of Fig. 11b and the rotated double triangle configuration of Fig. 11c, respectively, and a value of $\Delta\gamma_m \cdot FBW = 3.45$. For each figure, the polar plot labeled "a" illustrates the optimum variation with frequency and the plots labeled "b" or "c" illustrate the tapped delay line synthesized weights using two and three taps/element, respectively. Note the rather simple amplitude and phase variation of the optimum weights with frequency for the simple double triangle array, as compared to the rather complex variation obtained for the rotated double triangle. For the simple double triangle array, the resultant optimum and synthesized weights lie on the real axis for the scenario chosen. Because of this, it is difficult to assess from the polar plot quantitative differences between the optimum weights and the results for $N_t = 2$ and $N_t = 3$, as the data is compressed onto a line. However, a more detailed examination of this weight frequency variation shows a nearly monotonic variation with

55
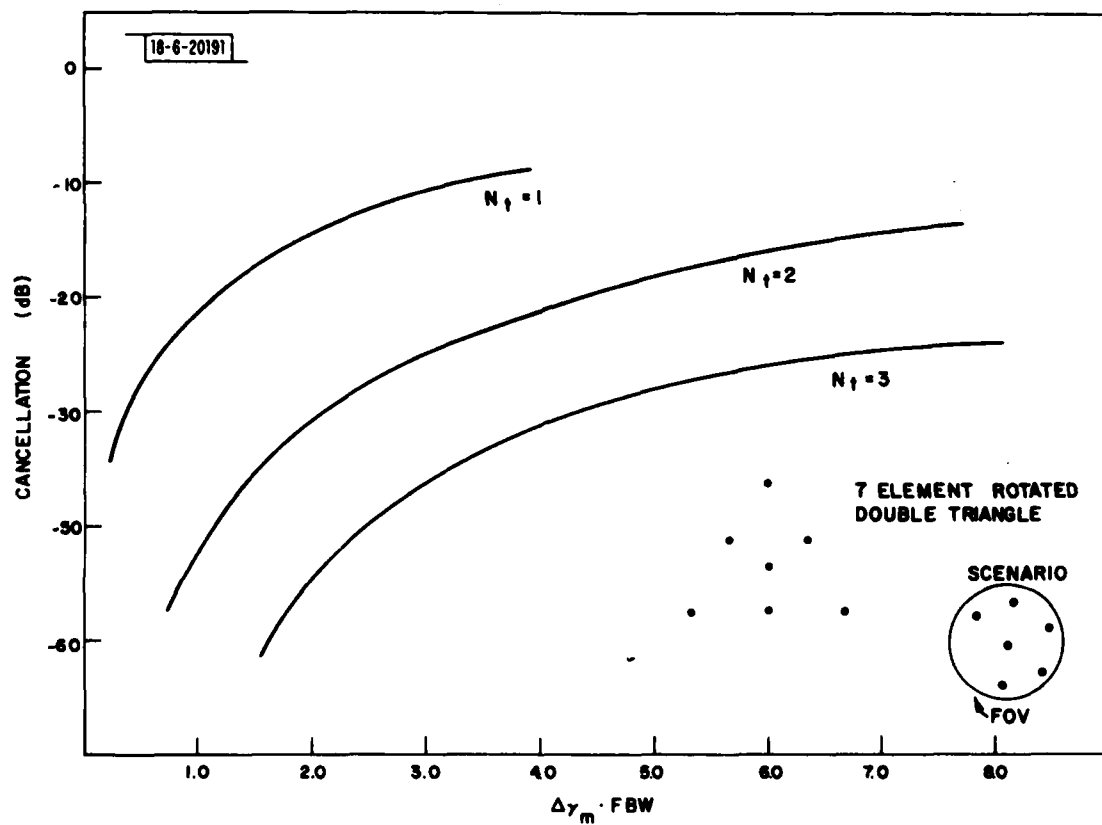
Fig. 17. Cancellation (dB) vs $\Delta\gamma_m \cdot$ FBW for the seven-element rotated double triangular array using a nearly-orthogonal six-source scenario as a function of the number of taps.
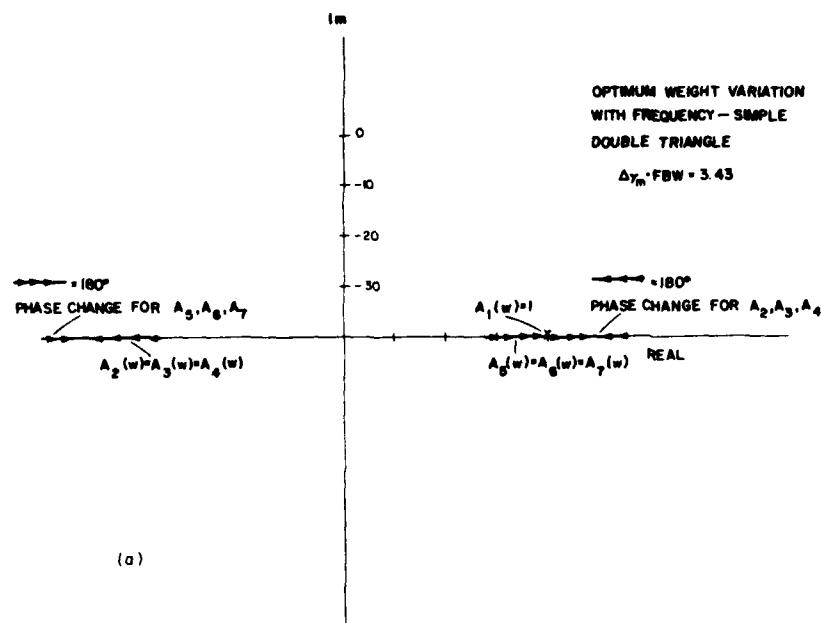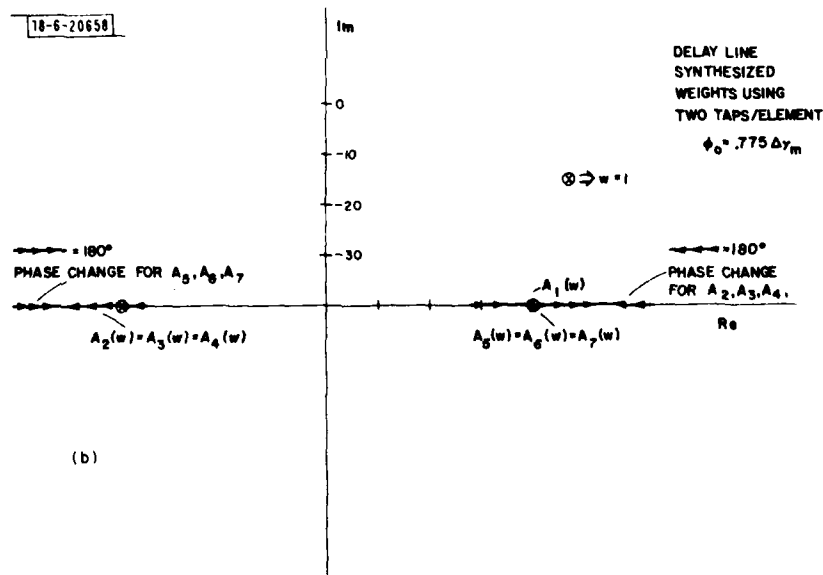
Fig. 18. Optimum weighting vs delay line synthesized weighting
for the seven-element simple-double triangular array using $\Delta\gamma_m$.
FBW = 3.43: (a) Optimum weight variation with frequency, (b) Delay
line synthesized weight variation with frequency for N_t = 2 and 3.
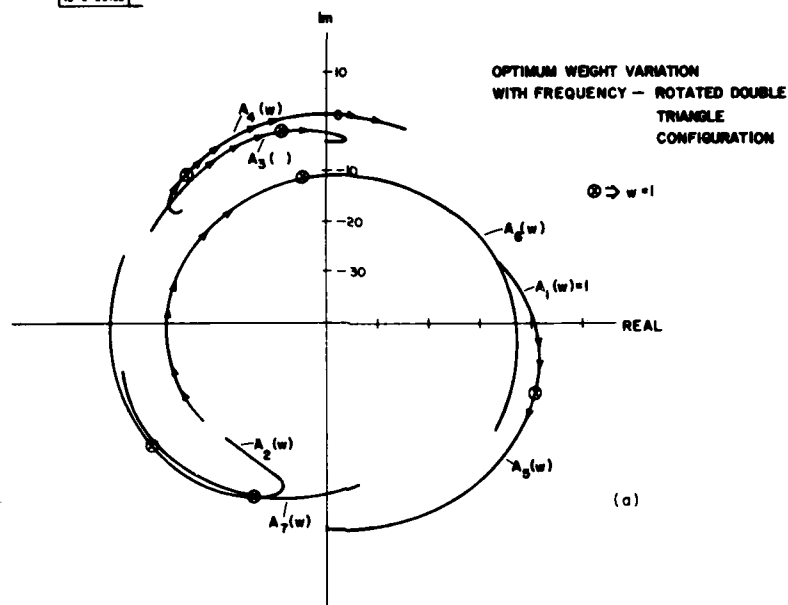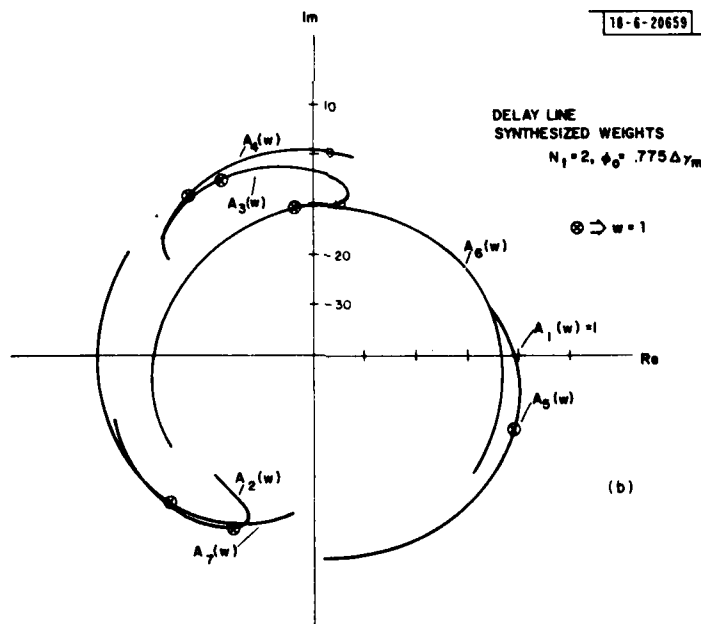
Fig. 19. Optimum weighting vs delay line synthesized weighting
for the seven-element rotated triangular array for $\Delta\gamma_m \cdot$ FBW = 3.43:
(a) Optimum weight variation with frequency, (b) Delay line synthe-
sized weight variation with frequency using N_t = 2.
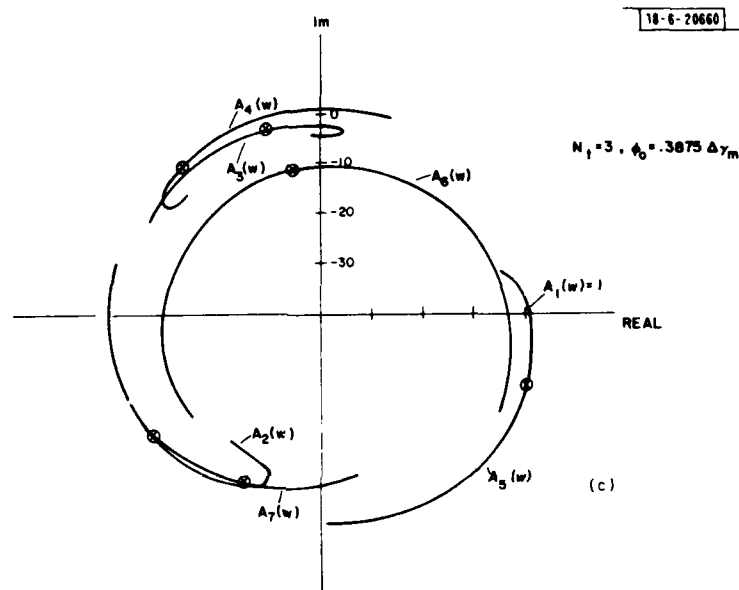
Fig. 19 (Continued). Optimum weighting vs delay line synthesized weighting for the seven-element rotated triangular array for $\Delta\gamma_m$. FBW = 3.43:   (c) $N_t = 3$.

frequency results for the simple double triangle array, as opposed to that corresponding to the rotated double triangle, for which some rather abrupt inflection points occur for the phase variation with frequency. As can be seen in Figs. 19b and c, using only two or three taps is not sufficient to precisely synthesize the rapid phase variation of the optimum weights of Fig. 19a, although the approximation to the optimum weights clearly improves as the number of taps increases. One might also compare the optimum weight variation with frequency for these two triangular array configurations to that of Fig. 13 for the three-element linear array, where the smooth behavior of the phase variation is again evident.

In order to pursue this point further, consider another 7-element array configuration characterized by six radial arms -- the hexagonal array illustrated in Fig. 11c. Six orthogonal source locations for this array can readily be determined and are illustrated in the insert of Fig. 20. The cancellation performance vs the parameter $\Delta\gamma_m \cdot$FBW is also plotted in this figure for a delay line employing either one, two or three taps/element. The tap spacing is, as before, chosen to be $\phi_0 = .775 \Delta\gamma_m$ for $N_t = 2$ and .3875 $\Delta\gamma_m$ for $N = 3$. We note the relatively narrowband nulling performance of this array is slightly worse than for the 7-element rotated double triangle array. As one might anticipate from the preceding results, the optimum weight variation with frequency also becomes rapidly varying as $\Delta\gamma_m \cdot$FBW increases. This is illustrated in Fig. 21, where we plot this weight variation vs frequency for $\Delta\gamma_m \cdot$FBW = 2.19. The optimum weight variation with frequency is plotted in Fig. 21a, along with the synthesized weight variation with frequency in Figs. 21b and c, respectively. Clearly, the same general comments pertaining to the rotated double triangle relative to Fig. 19 can be made for the hexagonal array. The inflection points present in the optimum weights phase variation occurs both near band-center and at the band edges.

For completeness, we briefly consider the two remaining array configurations of Fig. 11c: The square array and the pentagonal array, characterized by four and five radial arms, respectively. The cancellation performance for

Fig. 20. Cancellation (dB) vs $\Delta\gamma_m \cdot$ FBW for the seven-element hexagonal array using a six-source orthogonal scenario as a function of the number of taps.
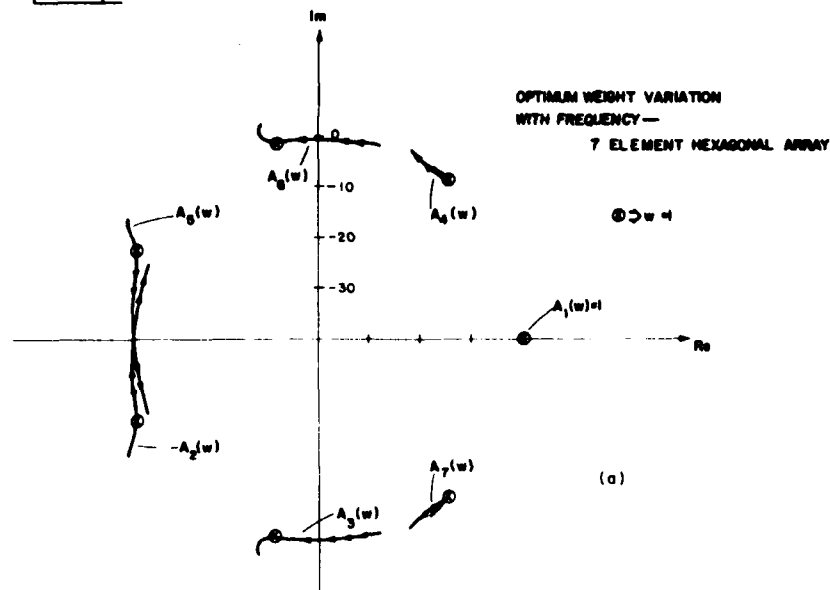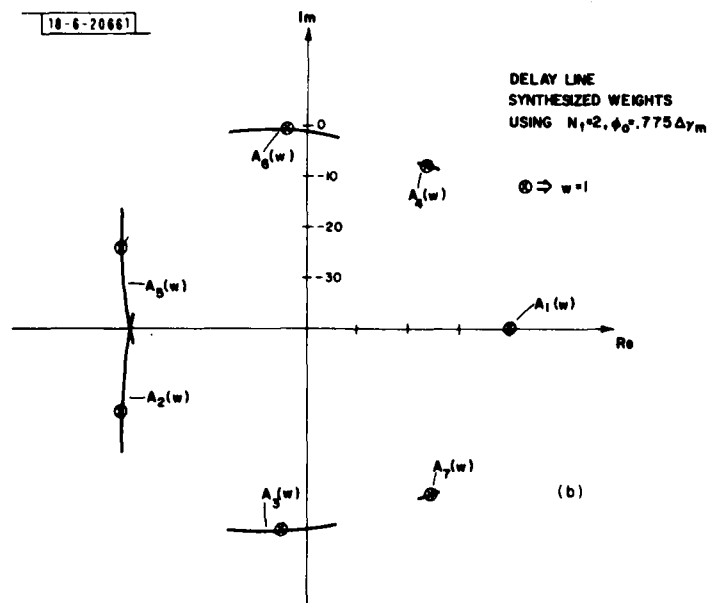
Fig. 21. Optimum weighting vs delay line synthesized weighting for
the seven-element hexagonal array for $\Delta\gamma_m \cdot$ FBW = 2.19: (a) Optimum
weight variation with frequency, (b) Delay line synthesized weight
variation with frequency using $N_t = 2$.

62
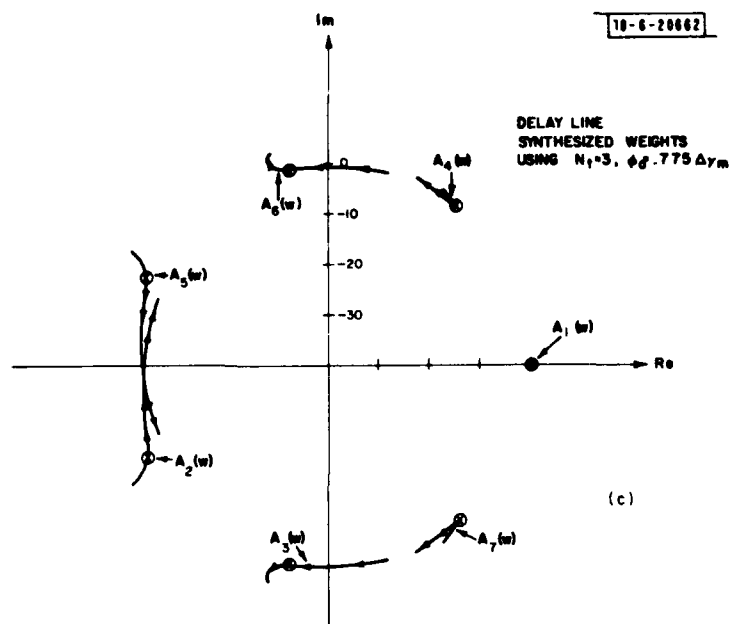
Fig. 21 (Continued). Optimum weighting vs delay line synthesized weighting for the seven-element hexagonal array for $\Delta\gamma_m$. FBW = 2.19: (c) $N_t = 3$.

these two arrays vs $\Delta\gamma_m \cdot$FBW is illustrated in Figs. 22 and 23, respectively. The nearly orthogonal source locations used in the simulation are illustrated in the insert of each figure. For comparison, we have presented results for two different orthogonal source scenarios for the 5-element square array, and included results using 4 taps/element for both arrays. When $N_t = 4$, we choose $\phi_0 = \Delta\gamma_m/4$. The results indicate performance similar to the other array types of Fig. 11c. Observe that notable improvement is obtained when 4 taps/element are used, and the results become comparable to the more simple linear and tri-angular arrays using two delay lines/element.

Finally, in order to bring together the results for all of the array types in Fig. 11, we examine the composite performance of the arrays obtained using a fixed number of taps/element. To accomplish this, we illustrate in Fig. 24a the collective performance of each array type vs $\Delta\gamma_m \cdot$FBW using frequency independent weights. Also sketched in the figure is the simple "rule of thumb" discussed in Section I (Fig. 1) used to assess the need for employing tapped delay lines. Note this rule of thumb curve serves as a useful upper bound on the composite set of cancellation results for the general class of arrays considered. Observe that for all of the array configurations, $C \propto (\Delta\gamma_m \cdot \text{FBW})^2$ -- i.e., for frequency independent weighting, array bandwidth performance degrades as the square of the parameter $2\pi \cdot \frac{D}{\lambda} \sin\Theta_m \cdot$FBW. This is a useful relationship to keep in mind in assessing array performance.

Fig. 24b illustrates the collective improvement of the 9 array types considered using $N_t = 2$. Observe a much larger spread in cancellation performance is obtained, indicating the improvement realized is somewhat sensitive to array configuration. However, the spread is narrow enough to enable one to estimate useful bounds on the anticipated improvement realized using $N_t = 2$ as a function of $\Delta\gamma_m \cdot$FBW. These bounds can be tabulated as a function of the desired cancellation level for a given number of taps. (Recall, all the above results were obtained assuming an earth coverage quiescent steering vector. Any other steering vector would increase or decrease the cancellation achieved by approximately the average quiescent gain to the interference sources rela-tive to earth coverage.) The result is illustrated in Table I. Fig. 24c

64
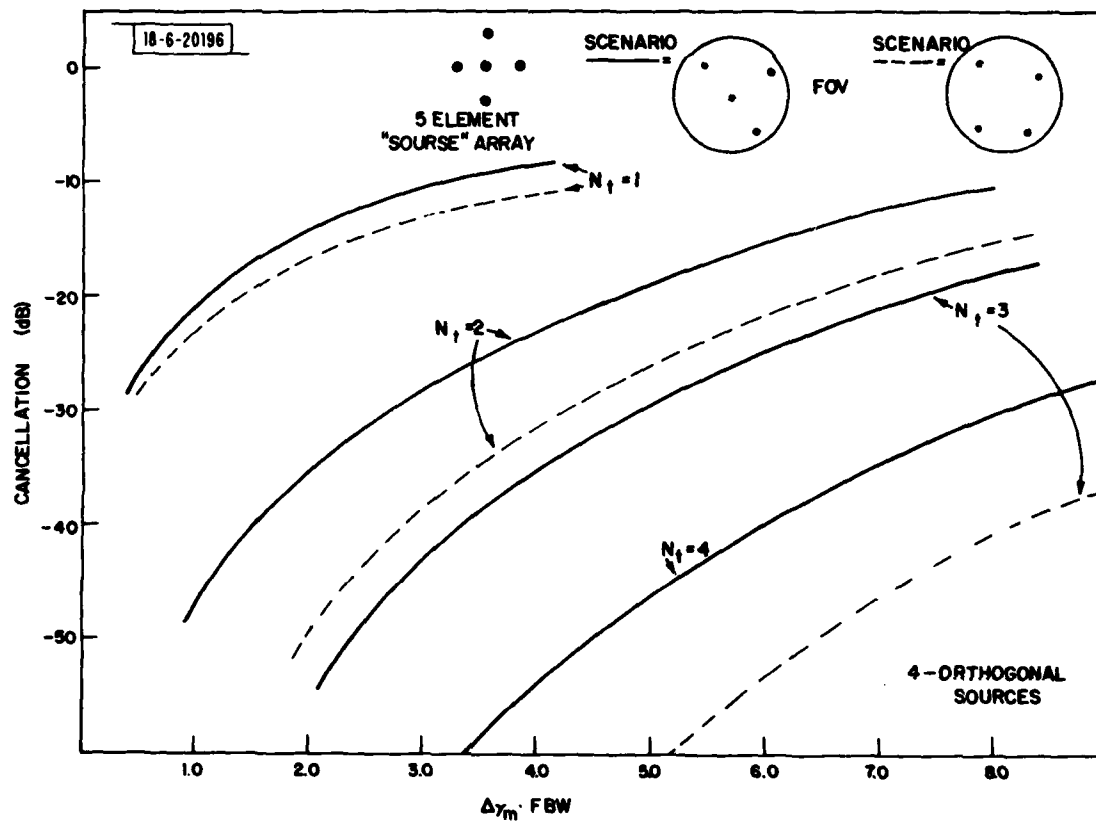
Fig. 22. Cancellation (dB) vs $\Delta\gamma_m \cdot$ FBW for the five-element square array using two-different four-source, nearly orthogonal scenarios as a function of the number of taps.
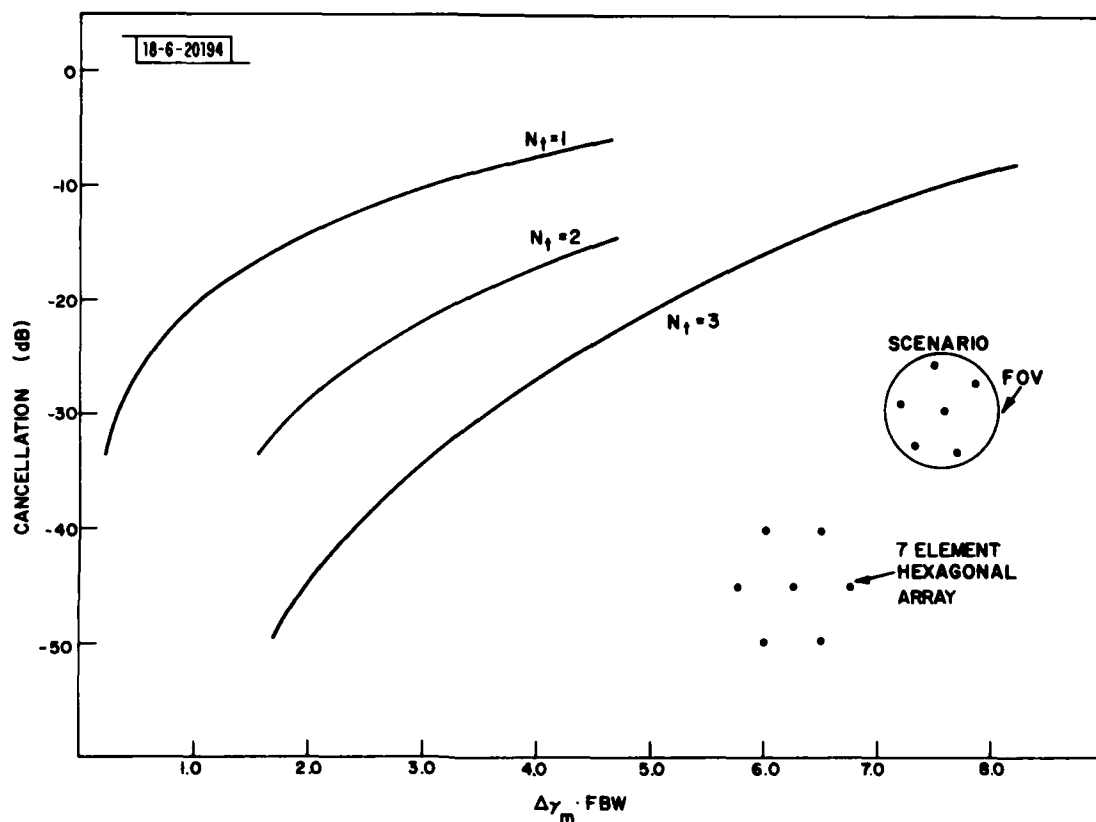
65
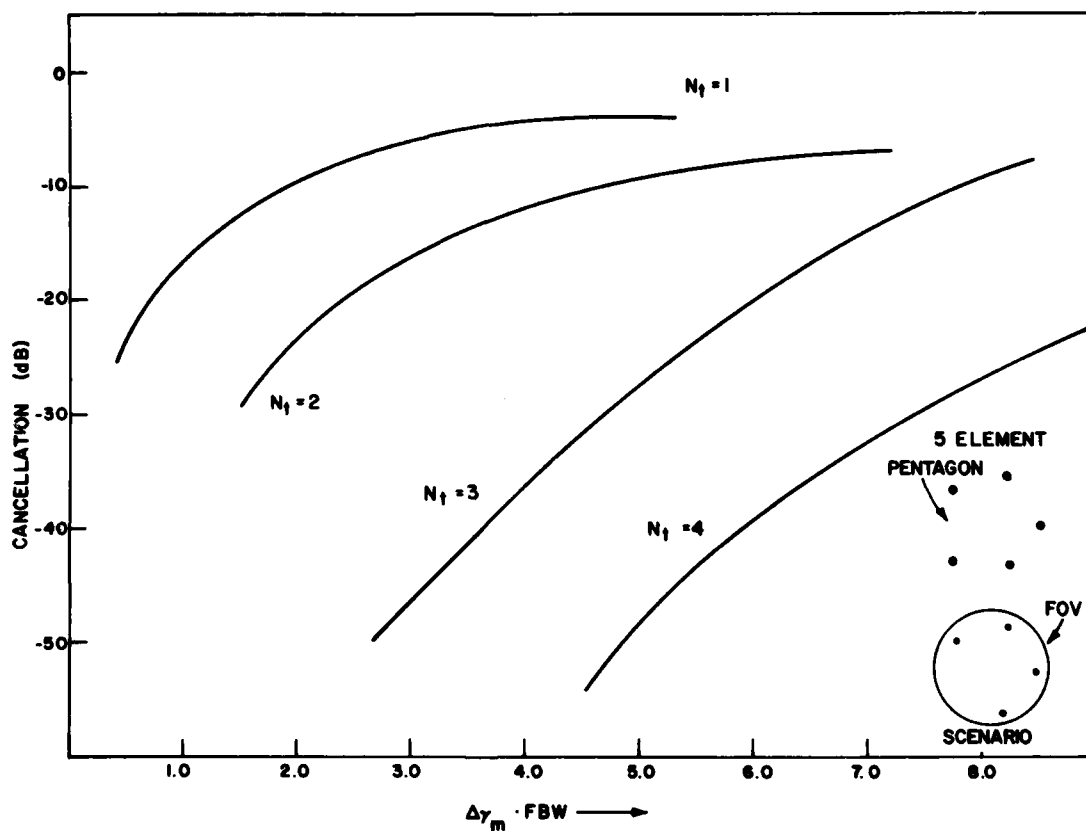
Fig. 23. Cancellation (dB) vs $\Delta\gamma_m \cdot$ FBW for the five-element pentagonal array using a four-source, nearly orthogonal scenario as a function of the number of taps.
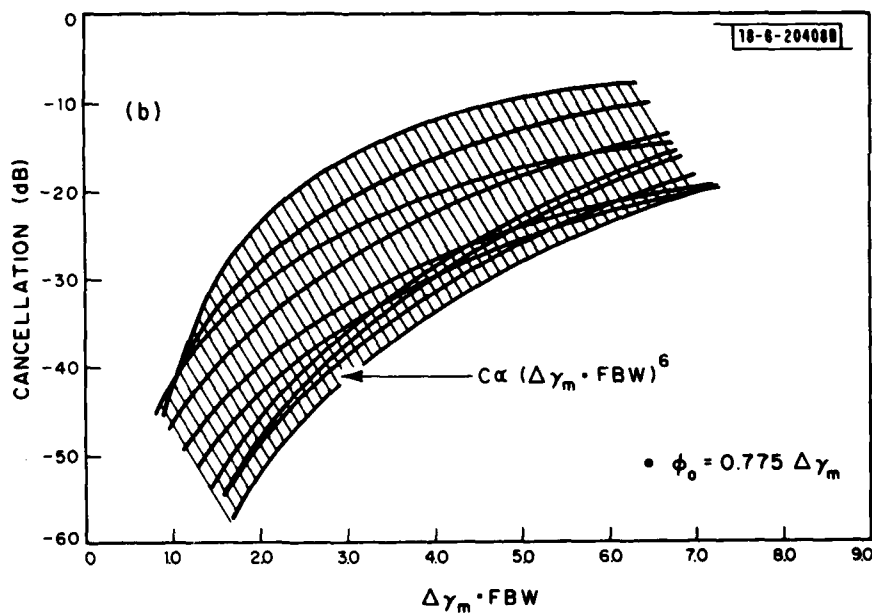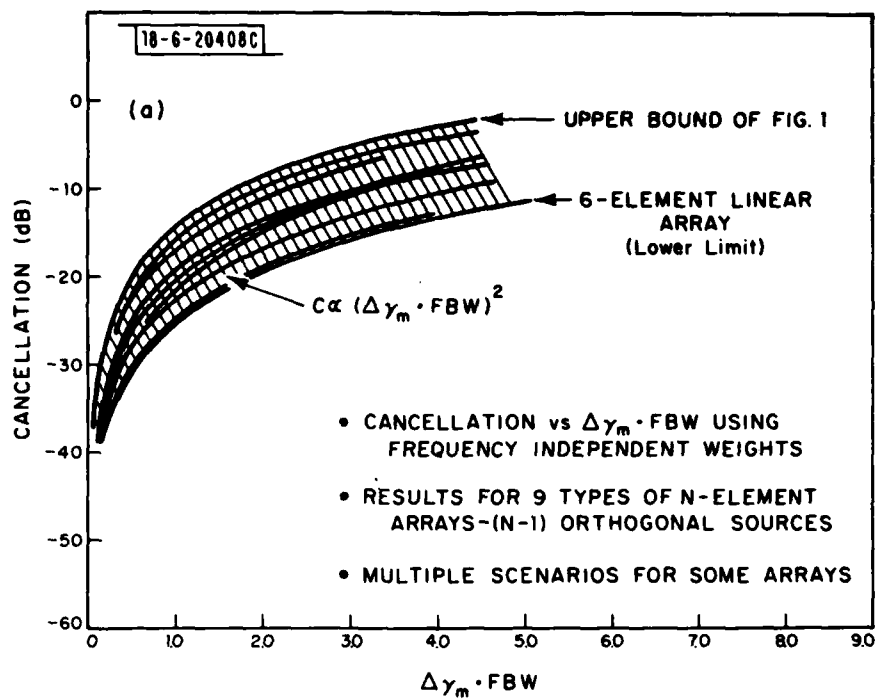
Fig. 24. Composite performance of the nine array configurations illustrated in Fig. 11: (a) Using frequency independent weighting, (b) Using delay line weighting with two taps/element.

67
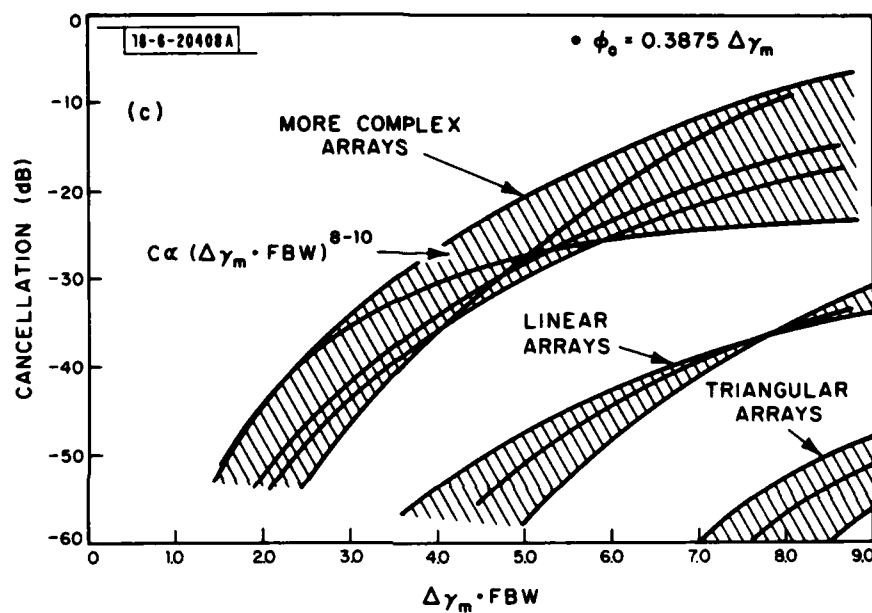
Fig. 24 (Continued). Composite performance of the nine array configurations illustrated in Fig. 11: (c) Using delay line weighting with three taps/element.

TABLE 1

COMPOSITE CANCELLATION BOUNDS vs N_t AND $X = \Delta\gamma_m \cdot FBW$ FOR THE NINE ARRAY
CONFIGURATIONS OF FIG. 11 ASSUMING AN EARTH COVERAGE QUIESCENT
RADIATION PATTERN

CANCELLATION (dB)	NUMBER OF TAPS	BOUND ON $\Delta\gamma_m \cdot FBW$
	$N_t = 1$	$X \leqslant 1.75$
-20	$N_t = 2$	$2.5 \leqslant X \leqslant 7.0$
	$N_t = 3$	$5 \leqslant X \leqslant 10$
	$N_t = 1$	$X \leqslant 0.6$
-30	$N_t = 2$	$1.5 \leqslant X \leqslant 4.75$
	$N_t = 3$	$3.5 \leqslant X \leqslant 5.0$
	$N_t = 1$	$X \leqslant 0.1$
-40	$N_t = 2$	$1.2 \leqslant X \leqslant 3.5$
	$N_t = 3$	$2.3 \leqslant X \leqslant 3.5$
	$N_t = 1$	---
-50	$N_t = 2$	$0.75 \leqslant X \leqslant 2.2$
	$N_t = 3$	$1.5 \leqslant X \leqslant 2.75$

69

illustrates the composite cancellation performance using N_t = 3. Observe that those classes of arrays categorized in Fig. 11 yield much different performance characteristics, offering support to the conjecture relating cancellation dependence on the number of taps to the spatial distributions of elements over the aperture. Results for N_t = 3 tabulated in Table 1 use the simulation data for the more complex arrays, i.e., the upper bound of Fig. 24c, which serves as a worst case estimate. Although the bounds are somewhat loose, they should prove useful in estimating a given array performance based on the given D/λ, field of view, and operating bandwidth.

V. DISCUSSIONS AND CONCLUSIONS

The results of Section IV indicate the cancellation performance of various types of planar arrays. It was determined that the cancellation potential of a particular array could be considered a function of the parameter $\Delta\gamma_m \cdot FBW$. Some physical insight into the interpretation of this parameter can be obtained in a qualitative manner by consideration of the time delays associated with the delay lines and the array. The maximum delay between the times of arrival of a plane wave at any pair of elements in an array of diameter D is given by

$$\tau_{MAX} = \frac{D \sin\Theta_m}{c} \qquad (45)$$

where c is the velocity of light. A perfect broadband weight would be capable of compensating for any time-delay from 0 to τ_{MAX} (see Eq. (18)). The choice of a total delay line length which gives a time delay of $775 \tau_{MAX}$ permits one, by appropriate weighting of the taps along the line, to approximate optimum weighting over this range relative to an arbitrary delay over the range $0 \leq \tau \leq \tau_{MAX}$. Simulations have shown the nulling performance to be not too sensitive to the value of total delay line length. For the case of 3 taps, we have somewhat arbitrarily chosen the tap spacing to be $\frac{.775 \ \tau_{MAX}}{2}$ = .3875 τ_{MAX}. For a larger number of taps, however, the appropriate spacing would appear to be τ_{MAX}/N_t, N_t being the number of taps. The choice of uniform tap spacing, while somewhat arbitrary, appears reasonable, given a fixed maximum length for the delay line. Such a uniform distribution of taps should permit most close approximation to any desired delay between 0 and τ_{MAX}.

The number of taps required to achieve a certain cancellation ratio depends on τ_{MAX} and on the fractional bandwidth. This dependence can be clarified by introducing the concept of a characteristic time, τ_0, defined as the inverse of the actual bandwidth in hertz; i.e.,

$$\tau_0 = \frac{1}{BW} \tag{46}$$

or, in terms of the fractional bandwidth FBW,

$$\tau_0 = \frac{\lambda}{c \cdot FBW} \tag{47}$$

The parameter τ_0 may be thought of, for example, as the width of the envelope of an RF pulse, the major frequency components of which lie within the spectrum BW. It is clear that in order for cancellation of such a pulsed waveform to occur, the pulse must appear simultaneously at the output of taps on more than one array element. For a two-element array, for example, the number of taps along a delay line of total length τ_{MAX} must be much greater than $\frac{\tau_{MAX}}{\tau_0}$ in order to be able to find such a coincidence of pulses at the array output for any angle of arrival up to θ_m.

(Using (45) and (47)), the parameter τ_{MAX}/τ_0 can be expressed as

$$2\pi \frac{\tau_{MAX}}{\tau_0} = \Delta\gamma_m \cdot FBW \tag{48}$$

Eq. (48), when interpreted relative to τ_{MAX}/τ_0, offers insight into the physical significance of the parameter $\Delta\gamma_m \cdot FBW$ used in plotting many of the curves in the report. For example, if only a single tap is used, it is reasonable to require $\tau_{MAX}/\tau_0 < .1$, or $\Delta\gamma_m \cdot FBW < .63$, and the curves in the report show poor cancellation for $\Delta\gamma_m \cdot FBW > .63$.

Other points that the authors wish to reiterate are that our analysis always assumes a maximally stressed array, i.e., an N-element array is always evaluated relative to N-1 orthogonal sources distributed over the FOV. This assumes that the array dedicates only a single spatial degree of freedom per source to be nulled.

A different approach to obtaining the capability of nulling N-1 sources over a wide band might be to use M >> N elements distributed over the same diameter D, but no tapped delay lines, so that many degrees of freedom could

72

be devoted to wideband nulling of each source. The disadvantage of this approach is that the nulls obtained are broader in angle, so that the nulling resolution is degraded, an effect that does not occur with the tapped delay-line approach. It also requires the physical deployment of many more elements than would be necessary with tapped delay lines. The tapped-delay line permits one to approximate the ideal narrowband weight at each frequency, and thus to maintain a high-resolution null (consistent with the resolving power of the antenna aperture) in a desired direction.

We have also shown that the number of taps required per array element depends not only on the parameter $\Delta \gamma_m \cdot$ FBW, but also on the geometry or shape of the array, more taps being required for more complex shapes. The number of taps is only weakly dependent on the number of elements that are placed inside the diameter D.

The analysis has been carried out using the Applebaum-Howells algorithm to obtain optimum tap weighting, but care has been taken to make the results of Section IV independent of the particular algorithm used. This has been done by choosing a large enough value of μ, the adaptive processor loop gain, and by choosing an appropriate quiescent weight vector, one which is guaranteed not to be orthogonal to the desired nulling weight vector.

In Table I in the last section of the report, we attempted to summarize the bandwidths achievable for 1, 2 and 3 taps at different cancellation levels. The table lists a range of values because of the above mentioned effect of dependence of the results on the shape of the array. This table can be used as a preliminary design guide, before more detailed analysis is carried out.

73

APPENDIX A

AN UPPER BOUND ON THE CANCELLATION ACHIEVABLE
USING FREQUENCY INDEPENDENT WEIGHTING

In this appendix, we develop the results leading up to Fig. 1 of the text, which serves as a qualitative estimate of the bandwidth potential of the N-element array antenna using frequency independent weights. Assume the presence of N-1 orthogonally located sources. Then Eq. (4) characterizing $\underline{\underline{R}}$ can be expanded in the form

$$\underline{\underline{R}} = \underline{\underline{R}}_0 + \Delta R = \underline{\underline{R}}_{1,0} + \cdots + \underline{\underline{R}}_{N-1,0} + \Delta \underline{\underline{R}}_1 + \cdots + \Delta \underline{\underline{R}}_{N-1} \tag{A1}$$

where $\underline{\underline{R}}_{j,0}$ denotes the zero-bandwidth correlation matrix of the jth source and $\Delta \underline{\underline{R}}_j$ the perturbation to $\underline{\underline{R}}_{j,0}$ due to non-zero bandwidth. The Nth eigenvalue s_N is given by

$$s_N = \underset{\underline{e}}{\text{Max}} \ \frac{\underline{e}^\dagger \cdot \underline{\underline{R}} \cdot \underline{e}}{\underline{e}^\dagger \cdot \underline{e}} = \underset{\underline{e}}{\text{Max}} \ \frac{\underline{e}^\dagger \cdot \Delta \underline{\underline{R}} \cdot \underline{e}}{\underline{e}^\dagger \cdot \underline{e}} \tag{A2}$$

where the maximization in (A2) is performed over all $\underline{e}$ orthogonal to the N-1 eigenvectors of $\underline{\underline{R}}_0$. Using a simple inequality, it follows that s_N can be bounded by

$$s_N \leq \sum_{j=1}^{N-1} \ \underset{\underline{e}}{\text{Max}} \ \frac{\underline{e}^\dagger \cdot \Delta \underline{\underline{R}}_j \cdot \underline{e}}{\underline{e}^\dagger \cdot \underline{e}} \tag{A3}$$

where no restriction is imposed on $\underline{e}$. Hence the maximum eigenvalue of each $\Delta \underline{\underline{R}}_j$ can be estimated, and s_N bounded by their sum. Consider $\Delta \underline{\underline{R}}_1$ and define $\gamma_{k,1} = \frac{k_0 D}{2} \sin\Theta_1 \ (x_k \cos\phi_1 + y_k \sin\phi_1)$. Then using Eq. (19) of the text, it follows that

$$(\Delta \underline{\underline{R}}_1)_{k,q} = \frac{E_0^2}{24} \ \text{FBW}^2 (\gamma_{k,1} - \gamma_{q,1})^2 \ e^{j(\gamma_{k,1} - \gamma_{q,1})} \tag{A4}$$

Δs_1, corresponding to the maximum eigenvalue of $\Delta \underline{\underline{R}}_1$, can be estimated by a simple bound on the elements of $\Delta \underline{\underline{R}}_1$. From Reference 4, it can be shown that

$$\Delta s_1 \leqslant \frac{E_0^2}{24} FBW^2 \quad (\frac{\pi D}{\lambda} \sin\Theta_1)^2 \; MAX \sum_{k=1}^{N} \sum_{q=1}^{N} (x_k - x_q)^2 \, e_k e_q^*$$

(A5)

$$\leqslant \frac{E_0^2}{24} \cdot FBW^2 \; (\frac{\pi D}{\lambda} \sin\Theta_1)^2 MAX \sum_{k=1}^{N} \sum_{q=1}^{N} (x_k - x_q)^2$$

If we assume an N-element, equi-spaced linear array geometry, then the maximum sum in (A5) can be determined. We obtain

$$MAX \sum_{k} \sum_{q} (x_k - x_q)^2 = \frac{2}{3} \frac{N(2N-1)}{N-1}$$

(A6)

Hence

$$\Delta s_1 \leqslant \frac{E_0^2}{24} FBW^2 \quad (\frac{\pi\Delta}{\lambda} \sin\Theta_1)^2 \frac{2}{3} \frac{N(2N-1)}{N-1}$$

(A7)

Then it follows from (A3) that $s_N \leqslant \Delta s_1 + \dots + \Delta s_{N-1}$, so that

$$s_N \leqslant \frac{E_0^2}{24} \quad \frac{1}{6} \frac{N(2N-1)}{N-1} (2\pi \cdot \frac{D}{\lambda} \cdot FBW)^2 \cdot [\sin^2\Theta_1 + \dots + \sin^2\Theta_{N-1}]$$

(A8)

Assume an earth coverage quiescent radiation pattern. The the quiescent interference-thermal noise ratio is simple $(N-1)G_e R_j$ if all N-1 interference sources are of equal power level. The adapted interference-thermal noise ratio is simply s_N. Hence, the cancellation C is given by

$$C \approx s_N / (N-1) G_e R_j$$

(A9)

Using Eq. (A8) in (A9) results in an upper bound on the achievable cancellation:

$$C \leqslant \frac{1}{16\pi^2} \frac{N \cdot (2N-1)}{(N-1)^2} \left(2\pi \cdot \frac{D}{\lambda} \cdot FBW\right)^2 \cdot [\sin^2\Theta_1 + \ldots + \sin^2\Theta_{N-1}]$$

(A10)

where the Θ_j, $j = 1,2, \ldots, N-1$, denote the positions of N-1 orthogonally positioned sources. Although the bound in Eq. (A10) is not generally tight, it serves as a worst case estimate of the bandwidth potential of the array. If the array diameter D/λ is large, so that grating lobes appear over the antenna FOV, then there are many angles Θ_j which satisfy the orthogonality condition defined by Eq. (2). Since aperture frequency dispersion is worse for sources positioned toward the edge of the FOV, we can obtain a good estimate of the worst case cancellation by choosing the Θ_j's uniformly distributed over the FOV, with one at the edge and the others at orthogonally located positions. In this case, Eq. (A10) can be expressed in the form

$$C \leqslant \frac{1}{16\pi^2} \frac{N(2N-1)}{(N-1)^2} \left(2\pi \cdot \frac{D}{\lambda} \sin\Theta_m \cdot FBW\right)^2 \left[1 + \frac{\sin^2\Theta_1}{\sin^2\Theta_m} + \ldots + \frac{\sin^2\Theta_{N-2}}{\sin^2\Theta_m}\right]$$

(A11)

If no grating lobes occur over the FOV, then the orthogonal positions $\Theta_1, \ldots, \Theta_{N-1}$ are uniquely specified; in this case Eq. (A11) will be weakly dependent on N. Fig. 1 illustrates the bound of Eq. (A11) for various values of N when the N-1 orthogonal source locations are assumed uniformly distributed over the FOV. The tightness of the bound in (A11) can be seen by comparison with simulations of the nine array configurations summarized in Fig. 24a.

APPENDIX B

EIGENVALUE AND EIGENVECTOR ANALYSIS FOR THE TWO-ELEMENT ARRAY
HAVING TWO TAPS/ELEMENT

In this Appendix, we outline the perturbation analysis leading up to Eqs. (23) and (24) characterizing the two-element array having two taps/element. The s_i and $\underline{e}_i$, $i = 1, \ldots, 4$ defined by Eq. (22) of the text can be estimated from $s_{1,0}$ and $\underline{e}_{i,0}$, which are the eigenvalues and eigenvectors of $\underline{\underline{R}}_0$, respectively. However, determining $\underline{e}_{2,0}$, $\underline{e}_{3,0}$ and $\underline{e}_{4,0}$ is complicated by the fact that the eigenvalue of $\underline{\underline{R}}_0$ are degenerate; i.e., $s_{1,0} = 2E_0^2$ and $s_{2,0} = s_{3,0} = s_{4,0} = 0$. Consequently, the corresponding eigenvectors of these degenerate eigenvalues are not unique. To circumvent this problem, we eliminate the ambiguity in the following manner. Define $\underline{u}_{1,0}$, $\underline{u}_{2,0}$, $\underline{u}_{3,0}$ and $\underline{u}_{4,0}$ to be a given orthonormal set of eigenvectors of $\underline{\underline{R}}_0$. The desired set of eigenvectors $\{\underline{e}_{i,0}\}$ can be expressed in terms of the $\underline{u}_{i,0}$ with the relating constants evaluated using Eq. (22a) of the text. Clearly, we must have $\underline{u}_{1,0} = \underline{e}_{1,0}$. $\underline{e}_{2,0}$ is chosen so that $s_2 = \text{MAX}\{\underline{e}_{2,0}^\dagger \cdot \Delta R \cdot \underline{e}_{2,0}\}$, where $\underline{e}_{2,0}$ is normalized to unity and $\underline{e}_{2,0}^\dagger \cdot \underline{e}_{1,0} = 0$. Given $\underline{e}_{2,0}$, $\underline{e}_{3,0}$ and $\underline{e}_{4,0}$ can be determined using a similar procedure. Once $\underline{e}_{3,0}$ and $\underline{e}_{4,0}$ are determined, then the $\underline{e}_i$ can be estimated from Eq. (22b). To this end, the eigenvector $\underline{e}_{2,0}$ is expanded in the form

$$\underline{e}_{2,0} = \underline{u}_{2,0} + k_3 \underline{u}_{3,0} + k_4 \underline{u}_{4,0} \tag{B1}$$

and the complex constants k_3 and k_4 are chosen so as to maximize the expression

$$\underset{k_3, k_4}{\text{MAX}} \quad \frac{\underline{e}_{2,0}^\dagger \cdot \Delta\underline{\underline{R}} \cdot \underline{e}_{2,0}}{\underline{e}_{2,0}^\dagger \cdot \underline{e}_{2,0}} \tag{B2}$$

$\underline{e}_{2,0}$ determined in this manner then yields directly the estimate s_2 for the second eigenvalue of $\underline{\underline{R}}$ given by Eq. (27a). Once $\underline{e}_{2,0}$ is determined, $\underline{e}_{3,0}$ and $\underline{e}_{4,0}$ can be determined from the linear combination

$$\underline{e}_{3,0} = d_2 \, \underline{u}_{2,0} + d_3 \, \underline{u}_{3,0} + d_4 \, \underline{u}_{4,0}$$

(B3)

$$\underline{e}_{4,0} = c_2 \, \underline{u}_{2,0} + c_3 \, \underline{u}_{3,0} + c_4 \, \underline{u}_{4,0}$$

where c_1, c_2, c_3 and d_1, d_2, d_3 are the complex constants. c_1, c_2, c_3, d_1, d_2 and d_3 are not independent but must satisfy the orthonormal conditions

$$\underline{e}_{2,0}^{\dagger} \cdot \underline{e}_{3,0} = \underline{e}_{3,0}^{\dagger} \cdot \underline{e}_{4,0} = \underline{e}_{4,0}^{\dagger} \cdot \underline{e}_{2,0} = 0$$

(B4)

$$\underline{e}_{2,0}^{\dagger} \cdot \underline{e}_{2,0} = \underline{e}_{3,0}^{\dagger} \cdot \underline{e}_{3,0} = \underline{e}_{4,0}^{\dagger} \cdot \underline{e}_{4,0} = 1$$

Eq. (B4) leads to the set of linear constraints

$$c_2 + k_3^* \, c_3 + k_4^* \, c_4 = 0$$

$$d_2 + k_3^* \, d_3 + k_4^* \, d_4 = 0$$

(B5)

$$c_2^* \, d_2 + c_3^* \, d_3 + c_4^* \, d_4 = 0$$

This set of equations can be simplified by arbitrarily choosing $d_2 = 0$, so that $\underline{e}_{3,0}$ is dependent only on $\underline{u}_{3,0}$ and $\underline{u}_{4,0}$ (that this is possible was determined in retrospect by considering $d_2 \neq 0$, and is due to our choice of the $\underline{u}_{k,0}$). After some manipulation, the expressions (B3) for $\underline{e}_{3,0}$ and $\underline{e}_{4,0}$ can be written in terms of $\underline{u}_{2,0}$, $\underline{u}_{3,0}$ and $\underline{u}_{4,0}$ in the form

$$\underline{e}_{3,0} = \frac{e^{-j\gamma_2}}{\sqrt{2}} \left[e^{j\gamma_2} \, \underline{u}_{4,0} - e^{j\gamma_1} \, \underline{u}_{3,0} \right]$$

(B6)

$$\underline{e}_{4,0} = \frac{e^{-j\gamma_2}}{\sqrt{2}\,\Delta} \left[e^{j\gamma_2} \, \underline{u}_{4,0} + e^{j\gamma_1} \, \underline{u}_{3,0} - \sqrt{2} \, \frac{\phi_0}{\Delta\gamma} \underline{u}_{2,0} \right]$$

(B7)

where $\Delta = \sqrt{\phi_0^2/\Delta\gamma^2}$. Eqs. (B6) and (B7) now form an orthonormal set of eigenvectors from which s_3, s_4 can be determined. It remains to choose the basis set $\{\underline{u}_{i,0}\}$. For our choice of basis functions, we choose

$$\underline{u}_{1,0}^{\dagger} = \frac{1}{2}\, [e^{-j\gamma_1},\ e^{-j\gamma_2},\ e^{j\phi_0}\, e^{-j\gamma_1},\ e^{j\phi_0}\, e^{-j\gamma_2}]$$

$$\underline{u}_{2,0}^{\dagger} = \frac{e^{-j\gamma_1}}{2}\, [1,\ -e^{+j\Delta\gamma},\ e^{+j\phi_0},\ -e^{j\phi_0}\, e^{-j\Delta\gamma}]$$

$$\underline{u}_{3,0}^{\dagger} = \frac{1}{\sqrt{2}}\, [1,\ 0,\ -e^{j\phi_0},\ 0] \tag{B8}$$

$$\underline{u}_{4,0}^{\dagger} = \frac{1}{\sqrt{2}}\, [0,\ 1,\ 0,\ -e^{-j\phi_0}]$$

Then Eq. (B6) for $\underline{e}_{3,0}$ used in (27a) yields s_3 and Eq. (B7) for $\underline{e}_{4,0}$ gives the estimate of s_4. Although this is not immediately clear, it can be shown by direct maximization of $\Delta\underline{R}$ of a linear combination $\underline{e} = \underline{e}_{3,0} = \alpha\underline{e}_{4,0}$, where α is the complex maximization parameter. Having determined $\underline{e}_{1,0}$, $\underline{e}_{2,0}$, $\underline{e}_{3,0}$ and $\underline{e}_{4,0}$ and s_1, s_2, s_3 and s_4, Eq. (27b) can be used to determine $\underline{e}_1$, $\underline{e}_2$, $\underline{e}_3$ and $\underline{e}_4$. However, due to the choice of $\underline{e}_{1,0}$, $\underline{e}_{2,0}$, $\underline{e}_{3,0}$ and $\underline{e}_{4,0}$, the sum in (22b) is zero since terms i=j are omitted. That is, $\underline{e}_{j,0}^{\dagger} \cdot \Delta R \cdot \underline{e}_{i,0} = 0$ when $j \neq i$, which is valid for all terms of $\Delta\underline{R}$ up to order FBW^6. Consequently, we have

$$\underline{e}_1 \approx \underline{e}_{1,0},\ \underline{e}_2 \approx \underline{e}_{2,0},\ \underline{e}_3 \approx \underline{e}_{3,0},\ \underline{e}_4 \approx \underline{e}_{4,0} \tag{B9}$$

where the $\underline{e}_{i,0}$ are determined as above by substituting (B8) into (B7). The results lead to Eq. (24) of the text.

ACKNOWLEDGMENT

REFERENCES

1.   B. Widrow, P. E. Mantey, L. J. Griffiths, and B. B. Goods, "Adaptive Antenna Systems," Proc. IEEE 55, 2143 (1967).

2.   W. E. Rodgers and R. T. Compton, Jr., "Adaptive Array Bandwidth with Tapped Delay-Line Processing," IEEE Trans. Aerospace Electronic Systems, AES-15, 21 (1979).

3.   A. M. Vural, "Effects of Perturbations on the Performance of Optimum/ Adaptive Arrays," IEEE Trans. Aerospace Electronic Systems, AES-15, 76 (1979).

4.   J. T. Mayhan and F. W. Floyd, "Factors Affecting the Performance of Adaptive Antenna Systems, and Some Evaluation Techniques," Technical Note 1979-14, Lincoln Laboratory, M.I.T. (to be published).

5.   W. F. Gabriel, "Adaptive Arrays - An Introduction," Proc. IEEE, 64, 271 (1976).

6.   J. T. Mayhan, "Bandwidth Limitations on Achievable Cancellation for Adaptive Nulling Systems," Technical Note 1978-1, Lincoln Laboratory, M.I.T. (17 February 1978) DDC AD-A054160.

7.   B. Friedman, Principles and Techniques of Applied Mathematics, (Wiley, New York, 1966).

REPORT DOCUMENTATION PAGE		READ INSTRUCTIONS BEFORE COMPLETING FORM
1. REPORT NUMBER ESD-TR-79-162	2. GOVT ACCESSION NO.	3. RECIPIENT'S CATALOG NUMBER
4. TITLE (and Subtitle) Wideband Adaptive Antenna Nulling Using Tapped Delay Lines		5. TYPE OF REPORT & PERIOD COVERED Technical Note
		6. PERFORMING ORG. REPORT NUMBER Technical Note 1979-45
7. AUTHOR(s) Joseph T. Mayhan William C. Cummings Alan J. Simmons		8. CONTRACT OR GRANT NUMBER(s) F19628-78-C-0002
9. PERFORMING ORGANIZATION NAME AND ADDRESS Lincoln Laboratory, M.I.T. P.O. Box 73 Lexington, MA 02173		10. PROGRAM ELEMENT, PROJECT, TASK AREA & WORK UNIT NUMBERS Program Element Nos. 63431F and 33126K Project No. 2029
11. CONTROLLING OFFICE NAME AND ADDRESS Air Force Systems Command, USAF Defense Communications Agency Andrews AFB 8th Street & So. Courthouse Road Washington, DC 20331 Arlington, VA 22204		12. REPORT DATE 26 June 1979
		13. NUMBER OF PAGES 90
14. MONITORING AGENCY NAME & ADDRESS (if different from Controlling Office) Electronic Systems Division Hanscom AFB Bedford, MA 01731		15. SECURITY CLASS. (of this report) Unclassified
		15a. DECLASSIFICATION DOWNGRADING SCHEDULE

16. DISTRIBUTION STATEMENT (of this Report)

Approved for public release; distribution unlimited.

17. DISTRIBUTION STATEMENT (of the abstract entered in Block 20, if different from Report)

18. SUPPLEMENTARY NOTES

None

19. KEY WORDS (Continue on reverse side if necessary and identify by block number)

wideband	tapped delay lines	eigenvectors
array	algorithms	covariance matrix
adaptive antenna	eigenvalues	adaptive weights
antenna nulling		

20. ABSTRACT (Continue on reverse side if necessary and identify by block number)

   For some applications, it is desirable to have an array antenna which can adaptively form antenna pattern "nulls" in the directions of a collection of interference sources. For large arrays operating over wide percentage bandwidths, some sort of frequency compensation is required at each array output port to accomplish broadband nulling. One technique commonly used is to employ a "tapped" delay line at each element output, with controllable weights (frequency independent) at the output of each tap. The objective of this report is to develop some insight into the way in which delay line compensation leads to improved performance, to develop some quantitative estimates of how performance varies with antenna and delay line parameters, and to develop some tools useful in the performance evaluation of frequency dependent weighting.

DD FORM 1473 EDITION OF 1 NOV 65 IS OBSOLETE
1 JAN 73

DA
FILM
5